



# Holocene climates of the Iberian Peninsula: pollen-based reconstructions of changes in the west–east gradient of temperature and moisture

Mengmeng Liu<sup>1</sup>, Yicheng Shen<sup>2</sup>, Penelope González-Sampériz<sup>3</sup>, Graciela Gil-Romera<sup>3</sup>, Cajo J. F. ter Braak<sup>4</sup>, Iain Colin Prentice<sup>1</sup>, and Sandy P. Harrison<sup>2</sup>

<sup>1</sup>Department of Life Sciences, Imperial College London, Silwood Park Campus, Buckhurst Road, Ascot, SL5 7PY, UK

<sup>2</sup>Geography & Environmental Science, Reading University, Whiteknights, Reading, RG6 6AH, UK

<sup>3</sup>Instituto Pirenaico de Ecología – CSIC, Avda. Montañana 1005, 50059, Zaragoza, Spain

<sup>4</sup>Biometris (Applied Mathematics and Applied Statistics Centre), Wageningen University & Research, 6708 PB, Wageningen, the Netherlands

**Correspondence:** Mengmeng Liu (m.liu18@imperial.ac.uk)

Received: 14 December 2021 – Discussion started: 20 December 2021

Revised: 13 January 2023 – Accepted: 9 February 2023 – Published: 5 April 2023

**Abstract.** The Iberian Peninsula is characterized by a steep west–east moisture gradient at present, reflecting the dominance of maritime influences along the Atlantic coast and more Mediterranean-type climate further east. Holocene pollen records from the Peninsula suggest that this gradient was less steep during the mid-Holocene, possibly reflecting the impact of orbital changes on circulation and thus regional patterns in climate. Here, we use 7214 pollen samples from 117 sites covering part or all of the last 12 000 years to reconstruct changes in seasonal temperature and in moisture across the Iberian Peninsula quantitatively. We show that there is an increasing trend in winter temperature at a regional scale, consistent with known changes in winter insolation. However, summer temperatures do not show the decreasing trend through the Holocene that would be expected if they were a direct response to insolation forcing. We show that summer temperature is strongly correlated with plant-available moisture ( $\alpha$ ), as measured by the ratio of actual evapotranspiration to equilibrium evapotranspiration, which declines through the Holocene. The reconstructions also confirm that the west–east gradient in moisture was considerably less steep during the mid-Holocene than today, indicating that atmospheric circulation changes (possibly driven by orbital changes) have been important determinants of the Holocene climate of the region.

## 1 Introduction

The Iberian Peninsula is characterized by a steep west–east gradient in temperature and moisture today, reflecting the dominance of maritime influences along the Atlantic coast and more Mediterranean-type climate further east. Projections of future climate change suggest that the region will become both warmer and drier, but nevertheless show that this west–east differentiation is maintained (Andrade et al., 2021a). The changes in temperature are projected to be larger and the occurrence of extreme temperature episodes more frequent in the south-central and eastern parts of Iberia than in Atlantic coastal areas (Carvalho et al., 2021). Similar gradients are seen in future projections of precipitation change, with the largest reductions in precipitation in the south-central region (Andrade et al., 2021b). However, the stability of these west–east gradients during the Holocene has been questioned. In particular, the west–east gradient in moisture appears to have been less pronounced during the mid-Holocene (8–4 ka) when cooler summers and wetter conditions in the Atlantic zone (e.g. Martínez-Cortizas et al., 2009; Mauri et al., 2015) coincided with the maximum development of mesophytic vegetation further east and south (Aranbarri et al., 2014, 2015; Carrión et al., 2010, 2009; González-Sampériz et al., 2017).

However, much of the evidence for Holocene climates of the Iberian Peninsula is based on qualitative interpre-

tations of vegetation changes, generally interpreted as reflecting changes in moisture availability (Morellón et al., 2018; Ramos-Román et al., 2018; Schröder et al., 2019). These records are extensive and they seem to indicate fairly complex spatial patterns of change. Kaufman et al. (2020) provides quantitative reconstructions of summer and winter temperature in their compilation of Holocene climate information, but there are only five terrestrial sites from the Iberian Peninsula. Iberia was also included in the quantitative pollen-based reconstructions of European climate through the Holocene in Mauri et al. (2015), which is an update of Davis et al. (2003). However, the geographical distribution of sites included is uneven and a large fraction of the records were from the Pyrenees and the Cantabrian mountains, with additional clustering of sites in coastal regions. Thus, the inferred patterns of climate over most of the central part of the peninsula are therefore largely extrapolated. Tarroso et al. (2016) have provided reconstructions of summer and winter temperature and mean annual precipitation since the Last Glacial Maximum for the Iberian Peninsula by using modern species distribution data to develop climate probability distribution functions (PDFs) and applying these to 31 fossil records. However, although they identified trends in precipitation during the Holocene, the temperature reconstructions do not seem to be reliable since they show no changes through time (9–3 ka), either for the Iberian Peninsula as a whole or for individual sub-regions, which is in contradiction to the other reconstructions. The current state of uncertainty about Holocene climate changes in Iberia is further exacerbated because quantitative reconstructions of summer temperature made at individual sites using chironomid data (Muñoz Sobrino et al., 2013; Tarrats et al., 2018) are not consistent with reconstructed summer temperatures based on pollen for the same sites.

We used the tolerance-weighted weighted averaging partial least squares regression with a sampling frequency correction (fxTWA-PLS) method introduced by Liu et al. (2020) as an improvement of the widely used weighted averaging partial least squares (WA-PLS; ter Braak and Juggins, 1993) method for reconstructing past climates from pollen assemblages. As presented in detail by Liu et al. (2020), this method is a more complete implementation of the theory underlying WA-PLS because it takes greater account of the climatic information provided by taxa with more limited climatic ranges and also applies a sampling frequency correction to reduce the impact of uneven sampling in the training data set. Liu et al. (2020) showed that fxTWA-PLS does indeed provide better reconstructions than WA-PLS. Here, we have further modified the algorithm implementing fxTWA-PLS, achieving an additional gain in performance. In the algorithm published by Liu et al. (2020), sampling frequencies were extracted from a histogram. In the modified algorithm, they are estimated using P-splines smoothing (Eilers and Marx, 2021), which makes the estimates almost independent of the chosen bin width (see Appendix A for de-

tails). In addition, the modified method applies the sampling frequency correction at two separate steps – the estimation of optima and tolerances and the regression step – a measure intended to produce more stable results. The modified method produces both improved  $R^2$  values and reduced compression and maximum bias in reconstructed climate variables (see Table A1, Figs. A1 and A2). We will return to this point in the Discussion.

We have used this improved method to reconstruct Holocene climates across Iberia, and re-examined the trends in summer and winter temperature and plant-available moisture, using a new and relatively comprehensive compilation of pollen data (Shen et al., 2022) with age models based on the latest radiocarbon calibration curve (IntCal20; Reimer et al., 2020). We explicitly test whether there are significant differences in the west–east gradient of moisture and seasonal temperatures through time. We then analyse the relationships between the changes in the three climate variables and how trends in these variables are related to external climate forcing. These analyses allow us to investigate whether the west–east gradient in moisture was less steep during the mid-Holocene and explore what controls the patterns of climate change across the region.

## 2 Methods

Multiple techniques have been developed to make quantitative climate reconstructions from pollen (see reviews in Bartlein et al., 2011; Chevalier et al., 2020; Salonen et al., 2011). Modern analogue techniques (MAT; Overpeck et al., 1985) tend to produce rapid shifts in reconstructed values corresponding to changes in the selection of the specific analogue samples, although this tendency is less marked in the conceptually analogous response surface technique (Bartlein et al., 1986). Regression-based techniques, including weighted averaging methods such as weighted averaging partial least squares (WA-PLS; ter Braak and Juggins, 1993), do not produce step changes in the reconstructions but suffer from the tendency to compress the reconstructions towards the central part of the sampled climate range. However, this tendency can be substantially reduced by accounting for the sampling frequency (fx) and the climate tolerance of the pollen taxa present in the training data set (fxTWA-PLS; Liu et al., 2020). Machine-learning and Bayesian approaches have also been applied to derive climate reconstructions from pollen assemblages (Peyron et al., 1998; Salonen et al., 2019). However, comparison of fxTWA-PLS with the Bayesian model BUMPER (Holden et al., 2017) shows that fxTWA-PLS performs better in capturing the climate of the modern training data set from Europe (Liu et al., 2020).

Although fxTWA-PLS has clear advantages over other quantitative reconstructions techniques, there is still a slight tendency towards compression. We have therefore made a further modification to the approach as described in Liu et al.

(2020). In the original version of fxTWA-PLS, the fx correction is applied as a weight with the form of  $1/\text{fx}^2$  in the regression (step 7 in Table 1 in Liu et al., 2020). Here (see Appendix A), we make a further modification of fxTWA-PLS by (a) applying the fx correction separately in both the taxon calculation and the regression (step 2 and step 7 in Table 1 in Liu et al., 2020) as a weight with the form of  $1/\text{fx}$  and (b) applying P-splines smoothing (Eilers and Marx, 2021) in order to reduce the dependence of the fx estimation on bin width. The modified version further reduces the biases at the extremes of the sampled climate range.

There are no generally accepted rules as to the choice of variables for palaeoclimate reconstruction. No systematic comparison of these choices has been made. However, it is widely understood that plant taxon distributions reflect distinct, largely independent controls by summer temperature, winter temperature and moisture availability (see e.g. Harrison et al., 2010). Therefore, in common with many other studies (Cheddadi et al., 1997; Jiang et al., 2010; Peyron et al., 1998; Wei et al., 2021; Zhang et al., 2007), we have chosen bioclimatic variables that reflect these independent controls, with mean temperature of the coldest month (MTCO) to represent winter temperature, mean temperature of the warmest month (MTWA) to represent summer temperature and  $\alpha$ , an estimate of the ratio of actual evapotranspiration to equilibrium evapotranspiration, to represent plant-available moisture. We choose not to use mean annual air temperature (MAAT) because it is a composite of summer and winter conditions; and we prefer to use an index of effective moisture availability (our estimate of  $\alpha$  being one such index) to mean annual precipitation (MAP), whose significance for plant function depends strongly on potential evaporation (a function of temperature and net radiation). Our calculation of  $\alpha$  takes account of this dependence. Growing degree days above a baseline of  $0^\circ\text{C}$  ( $\text{GDD}_0$ ) would be a possible alternative to MTWA as an expression of summer conditions but is most relevant as a predictor of “cold limits” of trees in cool climates, whereas MTWA better reflects the high-temperature stress on plants in Mediterranean-type climates.

We used the modified version of fxTWA-PLS to reconstruct these three climate variables. The individual and joint effects of MTCO, MTWA and  $\alpha$  were tested explicitly using canonical correspondence analysis (CCA). The modified version further reduces the biases at the extremes of the sampled climate range, while retaining the desirable properties of WA-PLS in terms of robustness to spatial autocorrelation (fxTWA-PLS; Liu et al., 2020).

The modern pollen training data set was derived from the SPECIAL Modern Pollen Data Set (SMPDS; Harrison, 2019). The SMPDS consists of relative abundance records from 6458 terrestrial sites from Europe, northern Africa, the Middle East and northern Eurasia (Fig. S1 in the Supplement) assembled from multiple different published sources. The pollen records were taxonomically standardized, and fil-

tered (as recommended by Chevalier et al., 2020) to remove obligate aquatics, insectivorous species, introduced species and taxa that only occur in cultivation (see Table S1 in the Supplement for the list). Taxa (mainly herbaceous) with only sporadic occurrences were amalgamated to higher taxonomic levels (genus, sub-family or family) after ensuring consistency with their distribution in climate space. As a result of these amalgamations, the SMPDS contains data on 247 pollen taxa. For our analysis, we use the 195 taxa that occur at more than 10 sites.

Modern climate data at each of the sites in the training data set were obtained from Harrison (2019). This data set contains climate reconstructions of MTCO, growing degree days above a baseline of  $0^\circ\text{C}$  ( $\text{GDD}_0$ ) and a moisture index (MI), defined as the ratio of annual precipitation to annual potential evapotranspiration. The climate at each site was obtained using geographically weighted regression (GWR) of the CRU CL v2.0 gridded data set of modern (1961–1990) surface climate at 10 arcmin resolution (New et al., 2002) in order to (a) correct for elevation differences between each pollen site and the corresponding grid cell and (b) make the resulting climate independent of the resolution of the underlying data set. The geographically weighted regression used a fixed bandwidth kernel of  $1.06^\circ$  ( $\sim 140\text{ km}$ ) to optimize model diagnostics and reduce spatial clustering of residuals relative to other bandwidths. The climate of each pollen site was then estimated based on its longitude, latitude and elevation. The MTCO and  $\text{GDD}_0$  were taken directly from the GWR and MI was calculated for each pollen site using a modified code from SPLASH v1.0 (Davis et al., 2017) based on daily values of precipitation, temperature and sunshine hours, again obtained using a mean-conserving interpolation of the monthly values of each. For this application, we used MTCO directly from the data set but calculated MTWA from MTCO and  $\text{GDD}_0$  based on the relationship between MTCO, MTWA and  $\text{GDD}_0$  given in Appendix 2 of Wei et al. (2021). We derived  $\alpha$  from MI following Liu et al. (2020). The modern training data set provides records spanning a range of MTCO from  $-42.4$  to  $14.8^\circ\text{C}$ , of MTWA from  $4.2$  to  $33.5^\circ\text{C}$  and of  $\alpha$  from  $0.04$  to  $1.25$  (Figs. 1 and S1).

The fossil pollen data from the Iberian Peninsula were compiled by Shen et al. (2022) and the data set was obtained from Harrison et al. (2022). The taxonomy used by Shen et al. (2022) is consistent with that employed in the SMPDS. Shen et al. (2022) provides consistent age models for all the records based on the IntCal20 calibration curve (Reimer et al., 2020) and the BACON Bayesian age-modelling tool (Blaauw et al., 2021; Blaauw and Christeny, 2011) using the supervised modelling approach implemented in the ageR package (Villegas-Diaz et al., 2021). We excluded individual pollen samples with large uncertainties (standard error larger than 100 years) on the ages attributed in the new age model. As a result, the climate reconstructions are based on a fossil data set of 7384 pollen samples from 117 records covering part or all of the last 12 000 years

**Table 1.** Details of the fossil pollen sites used. The fossil pollen data from the Iberian Peninsula were compiled by Shen et al. (2022) and obtained from <https://doi.org/10.17864/1947.000369>.

Site name	Entity name	Longitude (°E)	Latitude (°N)	Elevation (m)	Earliest sample (yr BP)	Latest sample (yr BP)	Length of record (yr)	No. of samples	No. of dating points	Source	Reference
Albufera Alcudia	ALCUDIA	3.12	39.79	0	7921	17	7904	54	4	EPD	Burjachs et al. (1994)
Algendar	ALGENDAR	3.96	39.94	21	8908	3816	5092	118	4	EPD	Yll et al. (1995, 1997)
Almenara de Adaja	ADAJA	-4.67	41.19	784	2830	477	2353	25	2	EPD	López-Merino et al. (2009b)
Alsa	ALSA	-4.02	43.12	560	4908	150	4758	24	3	EPD	Martiscal (1993)
Alvor Estuary	Abi 05/07	-8.59	37.15	1	7840	1699	6141	76	9	author	Schneider et al. (2010, 2016)
Ribeira do Farelo											
Ribeira da Torre											
Antas	ANTAS	-1.82	37.21	0	11141	4309	6832	95	6	EPD	Cano-Villanueva (1997), Pantaleón-Cano et al. (2003), Yll et al. (1995)
Arbarrain Mire	ARBARRAIN	-2.17	43.21	1004	6872	78	6794	91	8	author	Pérez-Díaz et al. (2018)
Arnacão de Pera	ADP 01/06	-8.34	37.11	2	7926	8	7918	17	7	author	Schneider et al. (2010, 2016)
Ribeira de Alcantarilha											
Armena	Armena	0.34	42.51	2238	5668	2217	3451	53	27	author	Leunda et al. (2019)
Arroyo de Aguas Frias	AGUASFRIAS	-5.12	40.27	1120	196	-41	237	50	5	author	Camarero et al. (2019)
Arroyo de las Cárcavas	CARCAVAS	-4.03	40.84	1300	2346	-57	2403	40	6	EPD	Morales-Molino et al. (2017a)
Arroyo de Navalacarta	NAVALACCA	-4.03	40.85	1250	706	-60	766	38	6	EPD	Morales-Molino et al. (2017a)
Arroyo de Valdeconejos	VALDECON	-4.06	40.86	1380	611	-56	667	44	8	EPD	Morales-Molino et al. (2017a)
Aixuri	ATXURI01	-1.55	43.25	500	6877	495	6382	33	2	EPD	Peñalba Garmendia (1989), Peñalba (1994)
Ayó de Vidriales	AYOO	-6.07	42.13	780	11846	-26	11872	63	15	EPD	Morales-Molino and García-Antón (2014)
Basa de la Mora	BSM08	0.33	42.55	1906	9856	184	9672	135	16	author	Pérez-Sanz et al. (2013)
Bassa Nera	BSN6	0.92	42.64	1891	9599	-55	9654	62	8	author	Garcés-Pastor et al. (2017)
Bermu Mire	BERMU	-4.15	39.43	783	1192	-25	1217	38	8	author	Luehmo-Lautenschlaeger et al. (2018c)
Borreguil de la Caldera	BdIC-01	-3.32	37.05	2992	1440	-56	1496	80	6	author	Ramos-Román et al. (2016)
Bosc dels Estanyons	BOSCESTA	1.63	42.48	2180	11761	26	11735	91	8	EPD	de Beaulieu et al. (2005), Miras et al. (2007)

Table 1. Continued.

Site name	Entity name	Longitude (°E)	Latitude (°N)	Elevation (m)	Earliest sample (yrBP)	Latest sample (yrBP)	Length of record (yr)	No. of samples	No. of dating points	Source	Reference
Botija Bog	BOTIJA	-4.7	39.6	755	3773	82	3691	25	4	author	Luelmo-Lautenschlaeger et al. (2018b)
Cala'n Porter	CPORTER	4.13	39.87	24	8809	4802	4007	86	4	EPD	Yll et al. (1997)
Cala Galdana	GALDANA	3.96	39.94	47	8498	4830	3668	101	5	EPD	Yll et al. (1994, 1995)
Campo Lameiro	PRD4	-8.52	42.53	260	11948	-11	11959	42	6	EPD	López-Merino et al. (2012)
Cañada de la Cruz	CANCRUZ	-2.69	38.07	1595	9413	-6	9419	39	14	EPD	Carrión et al. (2001a)
Canada del Gitano_Sierra de Baza	SBAZA	-2.7	37.23	1900	8460	103	8357	111	8	EPD	Carrión et al. (2007)
Canaleja	CANALEJA	-2.45	40.9	1029	11544	5515	6029	6	2	EPD	Cerrillo-Cuenca et al. (2007), Cerrillo-Cuenca and González-Cordero (2011)
Castello Lagoon	Castello Lagoon core EM	3.1	42.28	2	4944	307	4637	85	10	author	Ejarque et al. (2016)
Cha das Lameiras	LAMEIRAS	-7.68	40.94	950	11982	539	11443	32	8	author	López-Sáez et al. (2017)
Charco da Candieira	CANDIEIR	-7.58	40.34	1409	11970	32	11938	230	31	EPD	van der Knaap and van Leeuwen (1984, 1995, 1997)
Creixell	CreixellIT	1.43	41.16	1	6438	723	5715	32	2	EPD	Burjachs and Expósito (2015)
Cueto de la Avellanosa	CUETOAV	-4.36	43.12	1320	6969	292	6677	34	3	EPD	Mariscal-Álvarez (1983)
Culazón	CULAZON	-4.49	43.23	592	3895	-44	3939	69	11	EPD	López-Sáez et al. (2013)
El Brezosa	BREZOSA	-4.36	39.35	733	3958	-16	3974	68	11	author	Morales-Molino et al. (2018)
El Carrizal	CARRIZAL	-4.14	41.32	860	9851	0	9851	50	6	EPD	Franco-Múgica et al. (2005)
El Mañillo mire	MAI	-6.21	40.55	1100	10687	91	10596	104	10	EPD	Morales-Molino et al. (2013)
El Payo	ELPAYO	-6.77	40.25	1000	571	-56	627	50	6	EPD	Abel-Schaad et al. (2009b), Silva-Sánchez et al. (2016)
El Perro mire	ELPERRO	-4.76	39.05	690	4694	-69	4763	41	10	author	Luelmo-Lautenschlaeger et al. (2019a, b)
El Portalet	PORTALET	-0.4	42.8	1802	11838	2128	9710	207	13	author	González-Sampériz et al. (2006)
El Redondo	REDONDO	-5.66	40.22	1765	3222	31	3191	60	4	author	López-Sáez et al. (2016)
El Sabinar	SABINAR	-2.12	38.2	1117	6580	1140	5440	129	9	EPD	Carrión et al. (2004)
El Tiemblo	TIEMBLO	-4.53	40.36	1250	3184	3	3181	60	9	author	López-Sáez et al. (2018b)
Elix	ELX	-0.75	38.17	1	9903	3392	6511	79	4	EPD	Burjachs et al. (1997), Burjachs and Expósito (2015)
Enol	ENOL	-4.99	43.27	1075	10910	2487	8423	30	7	author	Moreno et al. (2011)
Es Grau	ESGRAU	4.26	39.95	2	7648	-13	7661	98	15	EPD	Burjachs et al. (2017)

Table 1. Continued.

Site name	Entity name	Longitude (°E)	Latitude (°N)	Elevation (m)	Earliest sample (yr BP)	Latest sample (yr BP)	Length of record (yr)	No. of samples	No. of dating points	Source	Reference
Espinosa de Cerrato	CERRATO	-3.94	41.96	885	11578	822	10756	157	7	author	Morales-Molino et al. (2017b), Múgica et al. (2001)
Estanilles	ESTANILLES	1.3	42.63	2247	11908	7646	4262	57	11	EPD	Pérez-Obiol et al. (2012)
Estanya Catena	Estanya Catena	0.53	42.03	677	11882	-37	11919	48	21	author	González-Sampériz et al. (2017), Morellón et al. (2011)
Fuente de la Leche	LECHE	-5.06	40.35	1382	2783	-18	2801	58	10	author	Robles-López et al. (2018)
Fuente del Pino Blanco	PINOBLANCO	-4.98	40.24	1343	653	-38	691	96	5	author	Robles-López et al. (2018)
Hinojos Marsh	HINOJOS	-6.39	36.96	2	4737	2682	2055	46	5	author	López-Sáez et al. (2018a)
Hort Timoner	HTIMONER	4.13	39.88	40	8686	5089	3597	46	4	EPD	Yll et al. (1997)
Hoya del Castillo	N-CAS	-0.16	41.48	258	10740	5629	5111	34	3	EPD	Davis and Stevenson (2007)
La Cruz	LACRUZ	-1.87	39.99	1024	1521	12	1509	23	2	EPD	Burjachs (1996)
La Molina mire	MOLINAES	-6.33	43.38	650	4482	388	4094	152	6	author	López-Merrino et al. (2011)
Labradillos Mire	LABRADILLOS	-4.57	40.34	1460	1447	184	1263	25	5	author	Robles-López et al. (2017a)
Lago de Ajo	LAGOAJO	-6.15	43.05	1570	11755	2175	9580	44	6	EPD	Allen et al. (1996), McKeever (1984)
Lagoa Comprida 2	LAGOA_CO	-7.64	40.36	1650	9863	94	9769	68	4	EPD	van den Brink and Janssen (1985), Janssen and Woldringh (1981), Moe and van der Knaap (1990)
Lagoa Travessa Mosca	TRAVESSI	-8.77	38.3	3	8174	3617	4557	65	4	EPD	Mateus (1985, 1989)
Laguna de la Mosca	LdImo composite	-3.31	37.06	2889	8344	-63	8407	68	18	author	Manzano et al. (2019)
Laguna de la Mula	LdIm 10-02	-3.42	37.06	2497	4581	-60	4641	32	8	author	Jiménez-Moreno et al. (2013)
Laguna de la Roya	LAROYA	-6.77	42.22	1608	11927	-41	11968	54	7	PANGAEA	Allen et al. (1996)
Laguna de Rio Seco	Laguna de Rio Seco core 1	-3.35	37.05	3020	10455	-54	10509	69	13	author	Anderson et al. (2011)
Laguna Guallar	N-GUA	-0.23	41.41	336	10654	8056	2598	30	6	EPD	Davis and Stevenson (2007)
Laguna Mesgosa	LAGMESAG	-2.81	41.97	1600	11981	-48	12029	90	5	EPD	von Engelbrechten (1998)
Laguna Negra	LAGNEGRA	-2.85	42	1760	11253	-48	11301	68	9	EPD	von Engelbrechten (1998)
Laguna Salada Chiperana	N-SAL	-0.17	41.23	150	6872	-40	6912	39	4	EPD	Valero-Garcés et al. (2000)

Table 1. Continued.

Site name	Entity name	Longitude (°E)	Latitude (°N)	Elevation (m)	Earliest sample (yr BP)	Latest sample (yr BP)	Length of record (yr)	No. of samples	No. of dating points	Source	Reference
Lake Banyoles	BANYOLES_1, Banyoles SB2	2.75	42.13	174	11952	3316	8636	141	15	EPD	Pérez-Obiol and Julià (1994), Revelles et al. (2015)
Lake Saloio	SALOIO	-9.02	39.61	70	2804	313	2491	24	2	EPD	Gomes (2011)
Lanzahíta	LANZBOG	-4.94	40.22	558	2657	-51	2708	51	8	author	López-Sáez et al. (1999, 2010)
Las Animas Mire	ANIMAS	-5.03	36.69	1403	797	-57	854	48	10	author	Alba-Sánchez et al. (2019)
Las Lanchas	LANCHAS	-4.89	39.59	800	374	-8	382	20	2	author	Luelmo-Lautenschlaeger et al. (2018a)
Las Pardillas	LASPARDI	-3.03	42.03	1850	10954	404	10550	74	4	EPD	Sanchez-Goñi and Hannon (1999)
Las Vinuelas	VINUELAS	-4.49	39.37	761	4210	-56	4266	58	9	author	Morales-Molino et al. (2019)
Les Palanques	PALANQUES	2.44	42.16	460	10011	524	9487	77	3	EPD	Revelles et al. (2018)
Manaderos	Manaderos core	-4.69	40.34	1292	1293	37	1256	59	9	author	Robles-López et al. (2020)
Marbore	Marbore composite	0.04	42.7	2612	11683	-18	11701	61	18	author	Leunda et al. (2017)
Monte Areo mire	AREO	-5.77	43.53	200	11547	-35	11582	55	12	EPD	López-Merino et al. (2010)
Montes do Buio Cuadramón	CUAII	-7.53	43.47	700	11347	241	11106	19	4	EPD	González and Saa (2000)
Navamuno	Navamuno_S3	-5.78	40.32	1505	11971	-28	11999	207	12	author	López-Sáez et al. (2020)
Navarrés	NAVAI, NAVARRE3	-0.68	39.1	225	11104	3131	7973	72	15	EPD	Carrion and Dupre (1996), Carrion and van Geel (1999)
Ojos del Tremendal	Ojos del Tremendal core 1	-2.04	40.54	1650	11875	1253	10622	52	4	author	Stevenson (2000)
Patateros bog	PATATERO	-4.67	39.6	700	2655	-19	2674	28	4	EPD	Dorado-Valiño et al. (2014a)
Pedrido	PEDRIDO	-7.07	43.44	770	5256	106	5150	71	30	EPD	Stefanini (2008)
Peña de Cadela	CADELA	-7.17	42.83	970	5233	-14	5247	91	9	EPD	Mighall et al. (2006)
Peña Negra	PENANEGR	-5.79	40.33	1000	3434	-62	3496	63	7	EPD	Abel-Schaad and López-Sáez (2013)
Pico del Sertal	SERTAL	-4.44	43.22	940	5200	106	5094	9	3	EPD	Mariscal-Álvarez (1986)
Pla de l'Estany	PLAESTANY	2.54	42.19	520	3577	-37	3614	43	4	EPD	Burjachs (1994)
Planell de Perafita	PERAFITA	1.57	42.48	2240	10244	-1	10245	56	11	EPD	Miras et al. (2010)
Posidonia Lligat	LLIGAT	-3.29	42.29	-3	779	15	764	32	5	EPD	López-Sáez et al. (2009)
Pozo de la Nieve	PozoN_2015 core	-4.55	40.35	1600	2258	-37	2295	41	10	author	Robles-López et al. (2017b)
Praïllos de Bossier Mire	BOSSIER	-4.07	36.91	1610	3428	4	3424	25	3	EPD	Abel-Schaad et al. (2017)

Table 1. Continued.

Site name	Entity name	Longitude (° E)	Latitude (° N)	Elevation (m)	Earliest sample (yr BP)	Latest sample (yr BP)	Length of record (yr)	No. of samples	No. of dating points	Source	Reference
Prat de Vila	PRATVILA	1.43	38.92	4	10776	538	10238	29	5	EPP	Burjachs et al. (2017)
Puerto de Belate	BELATE01	-2.05	43.03	847	8457	1746	6711	60	3	EPP	Penalba Garmendia (1989), Penalba (1994)
Puerto de las Estacas de Trueba	ESTACAS	-3.7	43.12	1160	6263	391	5872	9	3	PANGAEA	Martiscal (1989)
Puerto de Los Tornos	TORNOS01	-3.43	43.15	920	8718	-34	8752	47	4	EPP	Penalba Garmendia (1989)
Puerto de Serranillos	SERRANIL	-4.93	40.31	1700	2254	-50	2304	34	5	EPP	López-Merino et al. (2009a)
Quintanar de la Sierra	QUINTA02	-3.02	42.03	1470	11995	1953	10042	37	20	EPP	Penalba Garmendia (1989), Penalba (1994)
Roquetas de Mar	ROQUETAS	-2.59	36.79	0	6910	1057	5853	32	3	EPP	Cano-Villanueva (1997), Pantaleón-Cano et al. (2003), Pérez-Obiol et al. (1994), Yll et al. (1995)
Salada Pequeña	N-PEQ	-0.22	41.03	357	4350	669	3681	43	5	EPP	Davis (2010)
Saldropo	SALDROPO	-2.72	43.05	625	7577	403	7174	76	3	EPP	Penalba Garmendia (1989), Penalba (1994)
Salines playa-lake	SALINES	-0.89	38.5	475	11905	1394	10511	74	7	EPP	Burjachs et al. (2017)
San Rafael	SANRAFA	-2.6	36.77	0	10846	-30	10876	134	6	EPP	Cano-Villanueva (1997), Pantaleón-Cano et al. (2003), Yll et al. (1995)
Sanabria Marsh	SANABRIA	-6.73	42.1	1050	11832	0	11832	79	9	EPP	Allen et al. (1996), Hannon (1985), Turner and Hannon (1988)
Serra Mitjana Fen	MITJANA	1.58	42.47	2406	1490	412	1078	15	2	EPP	Miras et al. (2015)
Serranía de las Villuercas	VILLUERCAS	-5.4	39.48	1000	4156	128	4028	31	4	author	Gil-Romera et al. (2008)
Sierra de Gádor	GADOR	-2.92	36.9	1530	6222	1195	5027	86	6	EPP	Carrión et al. (2003)
Siles Lake	SILES	-2.5	38.4	1320	11527	189	11338	67	12	EPP	Carrión (2002)
Tubilla del Lago	TUB	-3.57	41.81	900	7436	31	7405	88	13	EPP	Morales-Molino et al. (2017b)
Turbera de La Panera Cabras	PANERA	-5.76	40.17	1648	164	-56	220	23	2	EPP	Abel-Schaad et al. (2009a)
Valdeyernos bog	VALDEYER	-4.1	39.44	850	3160	-60	3220	25	4	EPP	Dorado-Vaílino et al. (2014b)
Valle do Lobo Ribeira de Carcavai	VAL_PB2	-8.07	37.06	2	8331	16	8315	144	20	author	Schneider et al. (2010, 2016)
Verdeospesosa mine	VERDEOSPESOA	-2.86	43.06	1015	11137	0	11137	91	12	author	Pérez-Díaz and López-Sáez (2017)



Table 1. Continued.

Site name	Entity name	Longitude (°E)	Latitude (°N)	Elevation (m)	Earliest sample (yr BP)	Latest sample (yr BP)	Length of record (yr)	No. of samples	No. of dating points	Source	Reference
Vilamora Ribeira de Quarteira	Vilamora P01–5	−8.14	37.09	4	3851	919	2932	30	12	author	Schneider et al. (2010, 2016)
Villaverde	VILL-AVERDE	−2.37	38.8	870	8066	0	8066	104	9	EPD	Carrion et al. (2001b)
Xan de Llamas	XL	−6.32	42.3	1500	4113	34	4079	33	4	EPD	Morales-Molino et al. (2011)
Zoñar	ZONARcombined	−4.69	37.48	300	3234	−45	3279	52	17	author	Martin-Puertas et al. (2008)

(Fig. 2), with 42 individual records provided by the original authors, 73 records obtained from the European Pollen Database (EPD, <http://www.europeanpollendatabase.net>, last access: 10 March 2023) and 2 records from PANGAEA (<https://www.pangaea.de/>, last access: 10 March 2023). Details of the records are given in Table 1. The average temporal resolution of these records is 101 years. We then excluded a few samples where the reconstructed values of  $\alpha$  exceed the natural limit of 0 and 1.26. Finally, 7214 samples from 117 records are used for the analyses of the climate reconstructions. Summer and winter insolation are also calculated using the PAST software based on the age and latitude of each sample (Hammer et al., 2001).

Variance inflation factor (VIF) scores were calculated for both the modern climates and the climates reconstructed from fossil pollen records in order to avoid multicollinearity problems and thus guarantee that the climate variables (MTCO, MTWA,  $\alpha$ ) used here represent independent features of the pollen records.

In addition to examining the reconstructions for individual sites, we constructed composite curves for the Iberian Peninsula as a whole. The composite curves provide a way of comparing the relationship between trends in the reconstructed climate changes and insolation changes. The curves were constructed after binning the site-based reconstructions using  $\pm 500$ -year bins. We used 1000 bootstrap resamplings of the reconstructed climate values in each  $\pm 500$ -year bin to avoid the influence of a single value or a single site on the mean climate value in this bin, and used the standard deviation of the 1000 values to represent the uncertainty of the mean climate value. We constructed linear regression plots to examine the longitudinal and elevational patterns in the reconstructed climate variables and assessed the significance of differences in these trends through time compared to the most recent bin ( $0.5 \text{ ka} \pm 500$  years) based on  $p$  values, with the customary threshold of 0.05. We then compared the climate trends with changes in summer and winter insolation.

### 3 Results

The modified version of fxTWA-PLS reproduces the modern climate reasonably well (Table 2). The performance is best for MTCO ( $R^2$  0.75, RMSEP 4.70, slope 0.91) but is also good for  $\alpha$  ( $R^2$  0.68, RMSEP 0.16, slope 0.78) and MTWA ( $R^2$  0.57, RMSEP 3.47, slope 0.71). The correlations between pollen records and each of the three bioclimate variables, as assessed by CCA, were strong for both modern climate data and fossil reconstructions (Table 3). The variance inflation factor (VIF) scores are all less than 6, so there are no multicollinearity problems (Table 3) (Allison, 1994), making it possible to reconstruct all three climate variables independently based on pollen data. Furthermore, the taxa that contribute most strongly to reconstructing colder/warmer or wet-

**Table 2.** Leave-out cross-validation (with geographically and climatically close sites removed) fitness of the modified version of fxTWA-PLS for the mean temperature of the coldest month (MTCO), mean temperature of the warmest month (MTWA) and plant-available moisture ( $\alpha$ ), with P-splines smoothed fx estimation, using bins of 0.02, 0.02 and 0.002, respectively;  $n$  is the number of components used; Avg.bias is the average bias, while Max.bias is the maximum absolute bias and Min.bias is the minimum absolute bias; RMSEP is the root-mean-square error of prediction; and  $\Delta$ RMSEP is the per cent change rate of RMSEP, which is  $(\text{RMSEP}_n - \text{RMSEP}_{n-1})/\text{RMSEP}_{n-1}$  converted into percentage; when  $n = 1$ ,  $\text{RMSEP}_0$  is the RMSEP of the null model.  $p$  assesses whether using the current number of components is significantly different from using one component less, which is used to choose the last significant number of components (indicated in bold) to avoid over-fitting. The degree of overall compression is assessed by linear regression of the cross-validated reconstructions onto the climate variable;  $b_1$  and  $b_{1.se}$  are the slope and the standard error of the slope, respectively. The closer the slope ( $b_1$ ) is to 1, the less the overall compression is.

	$n$	$R^2$	Avg. bias	Max. bias	Min. bias	RMSEP	$\Delta$ RMSEP	$p$	$b_1$	$b_{1.se}$
MTCO	1	0.70	-0.86	25.23	0.00	5.20	-39.97	0.001	0.89	0.01
	2	0.73	-0.73	25.00	0.00	4.87	-6.29	0.001	0.91	0.01
	3	0.74	-0.71	24.38	0.00	4.86	-0.32	0.001	0.91	0.01
	<b>4</b>	<b>0.75</b>	<b>-0.59</b>	<b>24.27</b>	<b>0.00</b>	<b>4.70</b>	<b>-3.26</b>	<b>0.001</b>	<b>0.91</b>	<b>0.01</b>
	5	0.74	-0.63	34.54	0.00	4.77	1.51	1.000	0.91	0.01
MTWA	1	0.52	-0.29	17.13	0.00	3.72	-26.88	0.001	0.69	0.01
	2	0.56	-0.14	17.20	0.00	3.53	-5.06	0.001	0.71	0.01
	3	0.56	-0.13	17.01	0.00	3.53	-0.20	0.008	0.71	0.01
	<b>4</b>	<b>0.57</b>	<b>-0.11</b>	<b>17.30</b>	<b>0.00</b>	<b>3.47</b>	<b>-1.56</b>	<b>0.001</b>	<b>0.71</b>	<b>0.01</b>
	5	0.57	-0.11	17.34	0.00	3.48	0.10	0.780	0.71	0.01
$\alpha$	1	0.65	-0.014	0.787	0.000	0.165	-39.59	0.001	0.76	0.01
	2	0.68	-0.016	0.781	0.000	0.159	-3.55	0.001	0.77	0.01
	<b>3</b>	<b>0.68</b>	<b>-0.017</b>	<b>0.757</b>	<b>0.000</b>	<b>0.158</b>	<b>-0.61</b>	<b>0.023</b>	<b>0.78</b>	<b>0.01</b>
	4	0.69	-0.017	0.784	0.000	0.158	-0.43	0.108	0.79	0.01
	5	0.69	-0.017	0.850	0.000	0.158	0.26	0.985	0.80	0.01

ter/drier climates show predictable patterns consistent with their known ecological preferences (Table S2).

Winters were generally colder during the early to mid-Holocene than present, as shown by the coherent patterns of reconstructed anomalies at individual sites (Fig. 3a and d). Here, “present” means the most recent pollen bin (0.5 ka  $\pm$  500 years). The composite curve also shows a general increase in winter temperatures through time (Fig. 4a), consistent with the trend in winter insolation (Fig. 4d). The composite curve shows that it was ca. 4 °C cooler than today at 11.5 ka, but temperatures were only ca. 0.5 °C cooler than present after 2.5 ka. Winter temperatures today increase from north to south and are also affected by elevation; these patterns are still present in the Holocene reconstructions, but there is no spatial differentiation between western and eastern Iberia in the anomalies (Table 4, Fig. S2). The similarity of the changes compared to present geographically is consistent with the idea that the changes in winter temperature are driven by changes in winter insolation.

Summers were somewhat hotter than present in the west and cooler than present in the east during the early and mid-Holocene, as shown by the reconstructed anomalies at individual sites (Fig. 3b and e). This west–east difference could not arise if the changes in summer temperatures were a direct reflection of the insolation forcing (Fig. 4e). Indeed, the composite curve shows relatively little change in MTWA

(Fig. 4b), confirming that there is no direct relationship to insolation forcing (Fig. 4e).

There is a strong west–east gradient in  $\alpha$  at present (Fig. 2), with wetter conditions in the west and drier conditions in the east. However, the reconstructed anomalies at individual sites (Fig. 3c and f) suggest that the west was drier and the east was wetter than present in the mid-Holocene, resulting in a flatter west–east gradient. The west–east gradient is significantly different from the present between 9.5–3.5 ka (Fig. 5, Table 4), implying stronger moisture advection into the continental interior during the mid-Holocene. The change in gradient is seen in both high- and low-elevation sites (Fig. S3). There is also significant change in  $\alpha$  with elevation between 9.5–4.5 ka (Table 4, Fig. S4).

Summer temperatures are strongly correlated with changes in  $\alpha$ , both in terms of spatial correlations in the modern data set at a European scale and in terms of spatial and temporal correlations in the fossil data set from the Iberian Peninsula (Fig. 6). The patterns of reconstructed anomalies in MTWA and  $\alpha$  at individual sites are also coherent (Fig. 3b, c, e, and f), showing drier conditions and hotter summers in the west and wetter conditions with cooler summers in the east during the early to mid-Holocene. The west–east gradient in MTWA was significantly different from the present between 9.5 and 3.5 ka except 8.5 ka (Table 4, Fig. S5), roughly the interval when the gradient in  $\alpha$  was also significantly dif-

**Table 3.** Canonical correspondence analysis (CCA) result of modern and fossil-reconstructed MTCO, MTWA and  $\alpha$ . The summary statistics for the ANOVA-like permutation test (999 permutations) are also shown. VIF is the variance inflation factor, Df is the number of degrees of freedom,  $\chi^2$  is the constrained eigenvalue (or the sum of constrained eigenvalues for the whole model),  $F$  is significance and  $\text{Pr}(> F)$  is the probability. The CCA plots can be found in Fig. S11.

Axes		Axis 1	Axis 2	Axis 3	VIF
Constrained eigenvalues		0.3819	0.1623	0.1087	/
Correlations of the environmental variables with the axes:					
Modern	MTCO	−0.815	0.579	0.012	1.31
	MTWA	−0.700	−0.203	0.685	3.34
	$\alpha$	0.883	0.430	−0.187	3.39
		Df	$\chi^2$	$F$	$\text{Pr}(> F)$
Whole model		3	0.6530	78.113	0.001
MTCO		1	0.3082	110.597	0.001
MTWA		1	0.1602	57.489	0.001
$\alpha$		1	0.1846	66.252	0.001
CCA 1		1	0.3819	137.076	0.001
CCA 2		1	0.1623	58.252	0.001
CCA 3		1	0.1087	39.011	0.001
Axes		Axis 1	Axis 2	Axis 3	VIF
Constrained eigenvalues		0.3601	0.2266	0.2037	/
Correlations of the environmental variables with the axes:					
Fossil-reconstructed	MTCO	0.430	0.776	0.462	1.34
	MTWA	0.987	0.141	−0.076	5.40
	$\alpha$	−0.947	0.088	−0.308	5.28
		Df	$\chi^2$	$F$	$\text{Pr}(> F)$
Whole model		3	0.7905	226.98	0.001
MTCO		1	0.2465	212.34	0.001
MTWA		1	0.3298	284.07	0.001
$\alpha$		1	0.2142	184.53	0.001
CCA 1		1	0.3601	310.19	0.001
CCA 2		1	0.2266	195.24	0.001
CCA 3		1	0.2037	175.51	0.001

ferent from the present. Again, the change in the west–east gradient is registered at both high- and low-elevation sites (Fig. S6). However, there is no significant change in MTWA with elevation except at 8.5 and 7.5 ka (Table 4, Fig. S7).

#### 4 Discussion

The modified version of fxTWA-PLS (fxTWA-PLS2) (Tables 2 and A1) shows improved performance compared to the previous version (fxTWA-PLS1). Cross-validation  $R^2$  values are higher for MTCO and MTWA but almost unchanged for  $\alpha$ . The maximum bias is decreased for all three variables, especially for MTCO. The compression problem is also reduced for MTCO ( $b_1$  increases from 0.82 to 0.91) and MTWA ( $b_1$  increases from 0.69 to 0.71), while it remains roughly the same for  $\alpha$ . The overall performance statistics

thus show substantial improvements for MTCO and MTWA, while they show little change for  $\alpha$ . However, Fig. A1 shows that “non-physical” reconstructions beyond the natural limits of  $\alpha$  (0–1.26) are greatly reduced, especially at the lower limit. There are also fewer outliers in Figs. A1 and A2 for all three variables. Thus overall, the modified version further reduces the reconstruction biases, especially at the extremes of the sampled climate range. This improvement probably occurs because of the separate application of  $1/\text{fx}$  correction during both the calculation of optima and tolerances of taxa and during the regression step – instead of applying an overall weight of  $1/\text{fx}^2$  at the regression step, which can result in some extreme values (with low sampling frequency) being weighed too strongly and appearing as outliers.

The fxTWA-PLS2 reconstructions show that there was a gradual increase in MTCO over the Holocene, both for most

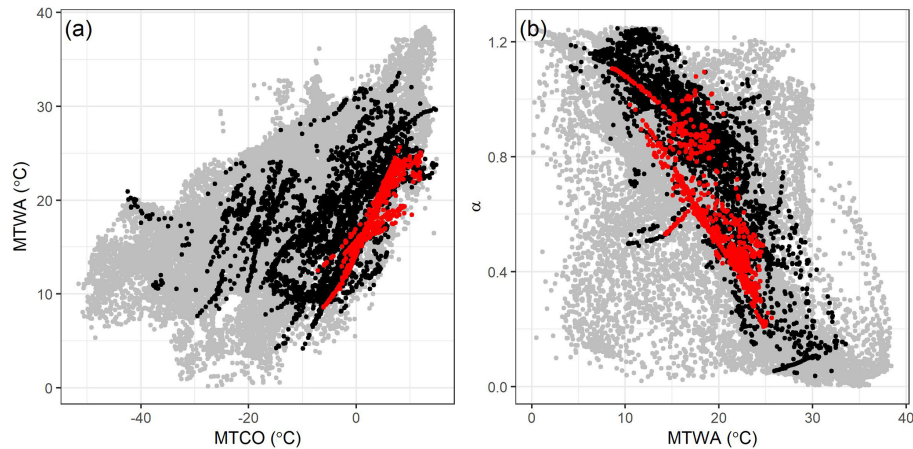


**Figure 1.** Climate space represented by mean temperature of the coldest month (MTCO), mean temperature of the warmest month (MTWA) and plant-available moisture as represented by  $\alpha$ , an estimate of the ratio of actual evapotranspiration to equilibrium evapotranspiration. The grey points show climate values for a rectangular area ( $21^{\circ}$  W– $150^{\circ}$  E,  $29^{\circ}$ – $82^{\circ}$  N) enclosing the SMPDS, derived from the Climate Research Unit CRU CL 2.0 database (New et al., 2002). The black points show climate values of the SMPDS. The red points show climate values of the Iberian Peninsula region in the SMPDS.

of the individual sites represented in the data set (Fig. 3) and for Iberia as a whole (Fig. 4). Colder winters in southern Europe during the mid-Holocene (6 ka) are a feature of many earlier reconstructions (e.g. Cheddadi et al., 1997; Wu et al., 2007). A general warming trend over the Holocene is seen in gridded reconstructions of winter season (December, January, February) temperatures as reconstructed using the modern analogue approach by Mauri et al. (2015), although there is somewhat less millennial-scale variability in these reconstructions (Fig. 7). Nevertheless, their reconstructions show a cooling of  $3^{\circ}\text{C}$  in the early Holocene, comparable in magnitude to the ca.  $4^{\circ}\text{C}$  cooling at 11.5 ka reconstructed here. They show a gradual warming trend through the Holocene but the differences from the present are very small (ca.  $0.5^{\circ}\text{C}$ ) after 2 ka, again consistent with our reconstructions of MTCO. Quantitative reconstructions of winter temperature for the five terrestrial sites from the Iberian Peninsula in the Kaufman et al. (2020) compilation all show a general trend of winter warming over the Holocene, but the magnitude of the change at some of the individual sites is much larger (ca.  $10^{\circ}\text{C}$ ) and there is no assessment of the uncertainty on these reconstructions. The composite curve of Kaufman et al. (2020) shows an increasing trend in MTCO through the Holocene, although with large uncertainties (Fig. 7). In contrast to the consistency of the increasing trend in MTCO during the Holocene between our reconstructions and those of Mauri et al. (2015) and Kaufman et al. (2020), there is no discernible trend in MTCO during the Holocene reconstruction of Tarroso et al. (2016). Indeed, there is no significant change in their MTCO values after ca. 9 ka, either for the peninsula as a whole (Fig. 7) or for any of the four sub-regions they considered. Our reconstructed trend in winter temperature is consistent with the changes

in insolation forcing at this latitude during the Holocene; it is also consistent with transient climate model simulations (Braconnot et al., 2019; Carré et al., 2021; Dallmeyer et al., 2020; Parker et al., 2021) of the winter temperature response to changing insolation forcing over the late Holocene in this region (Figs. 8 and S8). Thus, we suggest that changes in winter temperatures are a direct consequence of insolation forcing.

We have shown that there is no overall trend in MTWA during the Holocene (Fig. 4). According to our reconstructions, summer temperatures fluctuated between ca.  $0.5^{\circ}\text{C}$  above or below modern temperature. The lack of coherent trend in MTWA is consistent with the gridded reconstructions of summer (June, July, August) temperatures in the Mauri et al. (2015) data set and also with the five terrestrial sites from Iberia included in the Kaufman et al. (2020) data set. However, the patterns shown in the three data sets are very different from one another. Mauri et al. (2015) suggest the early Holocene was colder than today, and although temperatures similar to today were reached at 9 ka, most of the Holocene was characterized by cooler summers. Kaufman et al. (2020), however, showed warmer conditions during the early Holocene than at present, although they also show cooler conditions during the later Holocene. The differences between the three data sets could reflect differences in the reconstruction methods, or differences in the number of records used and in the geographic sampling. However, given the fact that all three data sets show similar trends in winter temperature, the lack of coherency between the data sets for MTWA points to there not being a strong, regionally coherent signal of summer temperature changes during the Holocene. Tarroso et al. (2016) also showed no significant changes in MTWA after ca. 9 ka (Fig. 7).

**Table 4.** Assessment of the significance of anomalies to 0.5 ka through time with longitude and elevation. The slope is obtained by linear regression of the anomaly onto the longitude or elevation; *p* is the significance of the slope (bold parts: *p* < 0.05); *x*<sub>0</sub> is the point where the anomaly is 0 in the linear equation, which indicates longitude or elevation where the anomaly changes sign.

	Age (ka)	Longitude (° E)			Elevation (km)		
		Slope	<i>p</i>	<i>x</i> <sub>0</sub>	Slope	<i>p</i>	<i>x</i> <sub>0</sub>
MTCO (° C)	0.5	0.00	/	/	0.00	/	/
	1.5	-0.07	0.411	-13.02	-0.30	0.411	-1.21
	2.5	-0.15	0.095	-8.56	-0.52	0.179	-0.40
	3.5	-0.13	0.314	-14.83	-0.81	0.142	-0.77
	4.5	-0.12	0.444	-17.28	-0.69	0.319	-1.46
	5.5	-0.24	0.247	-9.49	-0.61	0.503	-1.43
	6.5	-0.18	0.372	-12.74	-0.87	0.293	-0.88
	7.5	-0.15	0.421	-20.39	-1.38	0.080	-0.67
	8.5	-0.03	0.890	-77.87	-1.58	0.065	-0.10
	9.5	0.01	0.954	156.31	-1.79	0.060	0.11
	10.5	0.20	0.474	9.25	-1.38	0.241	-0.64
11.5	0.23	0.528	13.77	0.12	0.947	36.35	
MTWA (° C)	0.5	0.00	/	/	0.00	/	/
	1.5	-0.01	0.862	-26.38	-0.05	0.830	-3.35
	2.5	-0.09	0.137	-2.80	-0.45	0.092	1.19
	3.5	<b>-0.23</b>	<b>0.005</b>	<b>-2.03</b>	-0.40	0.284	1.74
	4.5	<b>-0.21</b>	<b>0.016</b>	<b>-2.01</b>	-0.58	0.126	1.55
	5.5	<b>-0.26</b>	<b>0.011</b>	<b>-2.43</b>	-0.49	0.280	1.53
	6.5	<b>-0.24</b>	<b>0.017</b>	<b>-2.30</b>	-0.62	0.137	1.41
	7.5	<b>-0.26</b>	<b>0.012</b>	<b>-3.02</b>	<b>-1.05</b>	<b>0.019</b>	<b>1.28</b>
	8.5	-0.24	0.061	-2.43	<b>-1.15</b>	<b>0.023</b>	<b>1.57</b>
	9.5	<b>-0.32</b>	<b>0.013</b>	<b>-3.20</b>	-0.44	0.459	1.34
	10.5	-0.18	0.115	-1.23	0.54	0.276	0.44
11.5	0.13	0.453	-7.25	0.37	0.663	0.22	
α	0.5	0.00	/	/	0.00	/	/
	1.5	0.00	0.508	8.99	-0.01	0.393	3.40
	2.5	0.00	0.517	-9.89	0.02	0.249	0.19
	3.5	<b>0.01</b>	<b>0.006</b>	<b>-4.91</b>	0.02	0.191	0.28
	4.5	<b>0.01</b>	<b>0.010</b>	<b>-4.60</b>	<b>0.05</b>	<b>0.008</b>	<b>0.79</b>
	5.5	<b>0.01</b>	<b>0.005</b>	<b>-4.75</b>	<b>0.05</b>	<b>0.027</b>	<b>0.67</b>
	6.5	<b>0.01</b>	<b>0.007</b>	<b>-5.34</b>	<b>0.06</b>	<b>0.004</b>	<b>0.60</b>
	7.5	<b>0.02</b>	<b>0.009</b>	<b>-6.05</b>	<b>0.09</b>	<b>0.000</b>	<b>0.75</b>
	8.5	<b>0.01</b>	<b>0.049</b>	<b>-6.67</b>	<b>0.09</b>	<b>0.000</b>	<b>0.88</b>
	9.5	<b>0.01</b>	<b>0.048</b>	<b>-6.40</b>	<b>0.07</b>	<b>0.012</b>	<b>0.70</b>
	10.5	0.01	0.183	-4.85	0.02	0.535	0.59
11.5	0.00	0.713	-2.76	0.03	0.654	0.93	

The chironomid record from Laguna de la Roya covers the late glacial and terminates at 10.5 ka (Muñoz Sobrino et al., 2013). The reconstructed July temperature during the early Holocene is ca. 12–13 °C, which is considerably cooler than today at this site. However, the authors caution that these samples have poor analogues and the record should be interpreted with caution. Chironomid-based reconstructions of July temperature at Basa de la Mora (Tarrats et al., 2018), a high-elevation site in the Pyrenees, indicate temperatures within ±0.5 °C of the modern climate during the early to mid-Holocene (10–6 ka), similar to our regional composite reconstructions. However, they show persistently cooler con-

ditions than present by ca. 1.5 °C between 4.5 and 2 ka, not seen in our reconstructions. Furthermore, a direct comparison of our reconstructions of MTWA at Basa de la Mora (Fig. S9) to the chironomid-based reconstructions highlights that the two records show very different trajectories, since the pollen-based reconstruction of this site shows a consistent warming trend throughout the Holocene. Although Tarrats et al. (2018) argue that discrepancies between their temperature reconstructions and pollen-based reconstructions reflect the fact that the vegetation of Iberia, including the mountain areas, is largely driven by moisture changes and perhaps is not a good indicator of temperature, we have shown that there

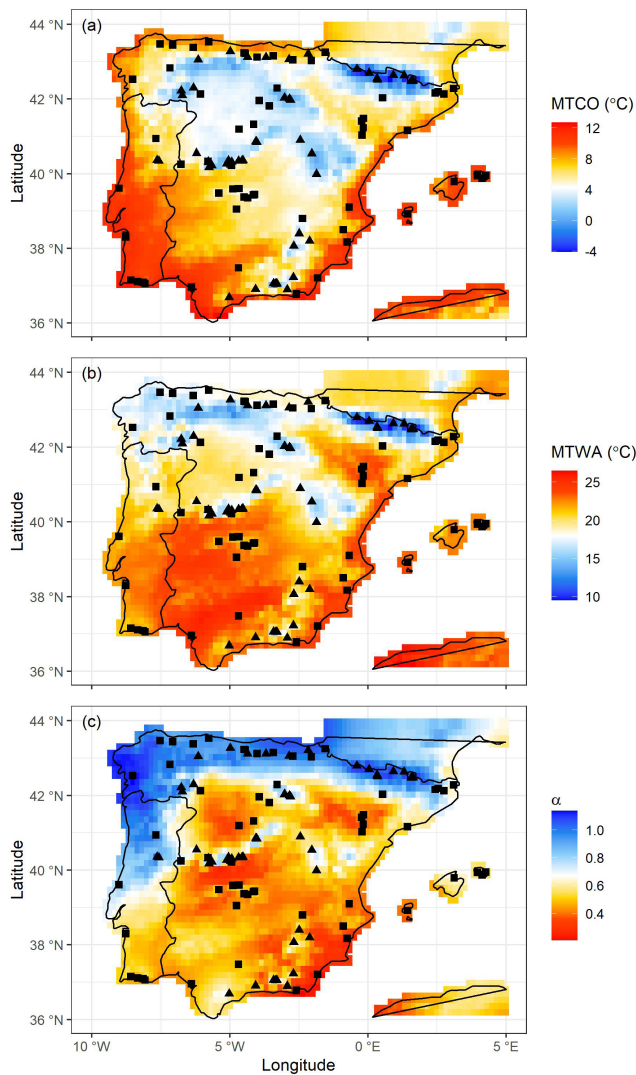


**Figure 2.** Map showing the location of the 117 fossil sites in the Iberian Peninsula used for climate reconstructions. Sites lower than 1000 m a.s.l. are shown as squares and sites higher than 1000 m a.s.l. are shown as triangles. The base maps show modern (a) mean temperature of the coldest month (MTCO), (b) mean temperature of the warmest month (MTWA) and (c) plant-available moisture as represented by  $\alpha$ , an estimate of the ratio of actual evapotranspiration to equilibrium evapotranspiration.

is sufficient information in the pollen records to reconstruct temperature and moisture independently (Tables 3 and S2). Thus, the cause of the differences between the pollen-based and chironomid-based reconstructions at Basa de la Mora is presumably related to methodology. In particular, the chironomid reconstructions use a training data set that does not include samples from the Pyrenees, or indeed the Mediterranean more generally, and may therefore not provide good analogues for Holocene changes at this site.

The lack of a clear trend in MTWA in our reconstructions (Fig. 4b) is not consistent with insolation forcing (Fig. 4e),

which shows a declining trend during the Holocene, nor is it consistent with simulated changes in MTWA in transient climate model simulations of the summer temperature response to changing insolation forcing over the Holocene in this region (Fig. 8). The change in moisture gradient during the mid-Holocene, however, suggests an alternative explanation whereby changes in summer temperature are a response to land-surface feedbacks associated with changes in moisture (Fig. 6). Specifically, the observed increased advection of moisture into eastern Iberia would have created wetter conditions there, which in turn would permit increased evapotranspiration, implying less allocation of available net radiation to sensible heating, and resulting in cooler air temperatures. Our reconstructions show that the west–east moisture gradient in mid-Holocene (Fig. 5) was significantly flatter than the steep moisture gradient today (Fig. 2), implying a significant increase in moisture advection into the continental interior during this period. Mauri et al. (2015) also showed that summers were generally wetter than at present in the east but drier than at present in the west in the early to mid-Holocene, supporting the idea of a flatter west–east gradient.

We have shown that stronger moisture advection is not a feature of transient climate model simulations of the Holocene, which may explain why these simulations do not show a strong modification of the insolation-driven changes in summer temperature (Fig. 8). Although the amplitude differs, all of the models show a general decline in summer temperature. The failure of the current generation of climate models to simulate the observed strengthening of moisture transport into Europe and Eurasia during the mid-Holocene has been noted for previous versions of these models (e.g. Bartlein et al., 2017; Mauri et al., 2014) and also shown in Fig. S8. Mauri et al. (2014), for example, showed that climate models participating in the last phase of the Coupled Model Intercomparison Project (CMIP5/PMIP3) were unable to reproduce reconstructed climate patterns over Europe at 6000 years BP and indicated that this resulted from oversensitivity to changes in insolation forcing and the failure to simulate increased moisture transport into the continent. Bartlein et al. (2017) showed that the CMIP5/PMIP3 models simulated warmer and drier conditions in mid-continental Eurasia at 6000 years BP, inconsistent with palaeoenvironmental reconstructions from the region, as a result of the simulated reduction in the zonal temperature gradient, which resulted in weaker westerly flow and reduced moisture fluxes into the mid-continent. They also pointed out the strong feedback between drier conditions and summer temperatures. The drying of the mid-continent is also a strong feature of the mid-Holocene simulations made with the current generation of CMIP6/PMIP4 models (Brierley et al., 2020). The persistence of these data–model mismatches highlights the need for better modelling of land-surface feedbacks on atmospheric circulation and moisture.

There are comparatively few pollen-based reconstructions of moisture changes during the Holocene from Iberia.

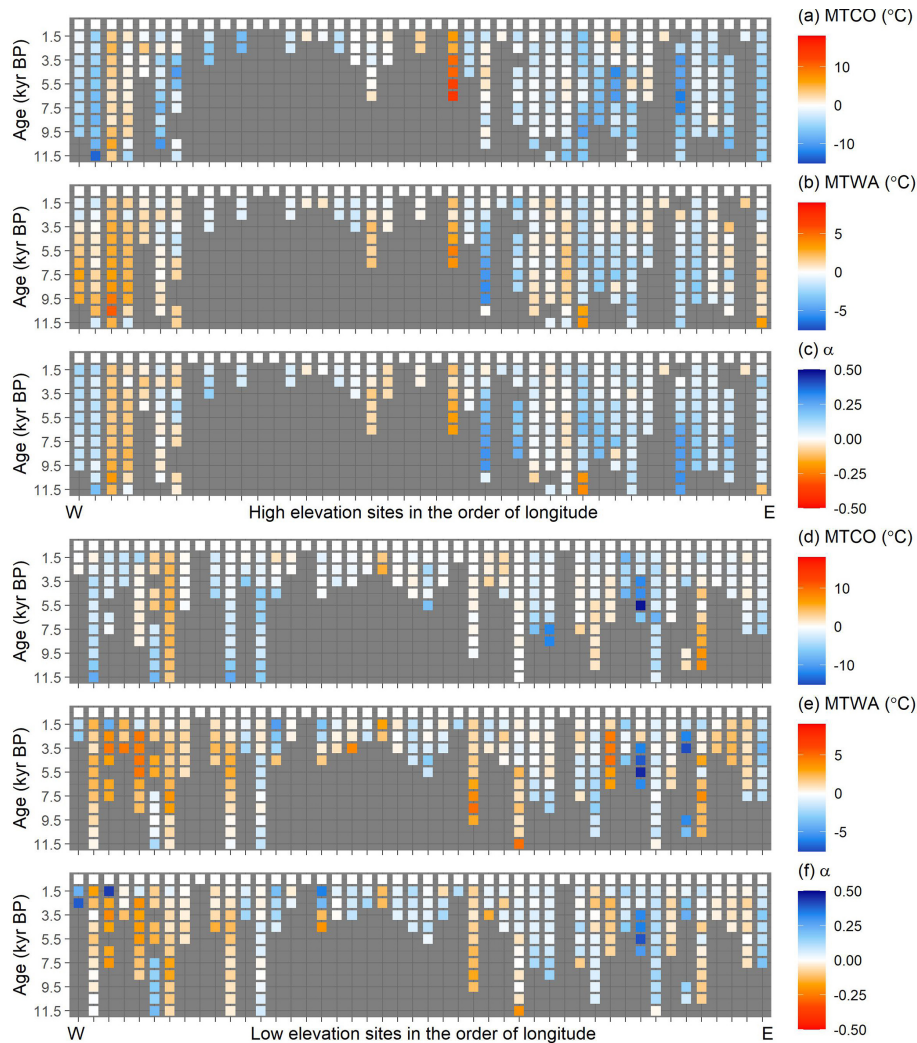


**Figure 3.** Reconstructed anomalies in climate at individual sites through time. The sites are grouped into high- (> 1000 m) and low- (< 1000 m) elevation sites and organized from west to east. Grey cells indicate periods or longitudes with no data. The individual plots show the anomalies in reconstructed (a, d) mean temperature of the coldest month (MTCO), (b, e) mean temperature of the warmest month (MTWA) and (c, f) plant-available moisture as represented by  $\alpha$ , an estimate of the ratio of actual evapotranspiration to equilibrium evapotranspiration. The anomalies are expressed as deviations of the mean value in each bin ( $\pm 500$  years) from the most recent bin ( $0.5 \text{ ka} \pm 500$  years) at each site.

Records from Padul show increased mean annual and winter precipitation during the early and mid-Holocene (Camuera et al., 2022; García-Alix et al., 2021). Reconstructions of mean annual and winter precipitation (Camuera et al., 2022) and the ratio of annual precipitation to annual potential evapotranspiration (Wei et al., 2021) also show wetter conditions at this time at El Cañizar de Villarquemado. Both of these sites lie in the eastern part of the Iberian Peninsula, so these reconstructions are consistent with our interpretation of wetter conditions in this region during the interval between 9.5 and 3.5 ka. Ilvonen et al. (2022) provide pollen-based reconstructions of mean annual, summer and winter precipitation from eight sites in Iberia, using WA-PLS and a Bayesian modelling approach. Although they focus on the

contrasting pattern of hydroclimate evolution between northern and southern Iberia, the three easternmost sites (San Rafael, Navarres and Quintanar de la Sierra) show much wetter conditions during the early to mid-Holocene. With the exception of the record from Monte Areo, the records from further west are relatively complacent and indeed two sites (Zalamar, El Maillo) show decreased precipitation between 8 and 4 ka. Thus, these records are consistent with our interpretation that the west–east gradient of moisture was reduced between 9.5 and 3.5 ka (Fig. 5).

Speleothem oxygen-isotope data from the Iberian Peninsula provide support for our pollen-based reconstructions of changes in the west–east gradient of moisture through the Holocene. The speleothem records show a progressive

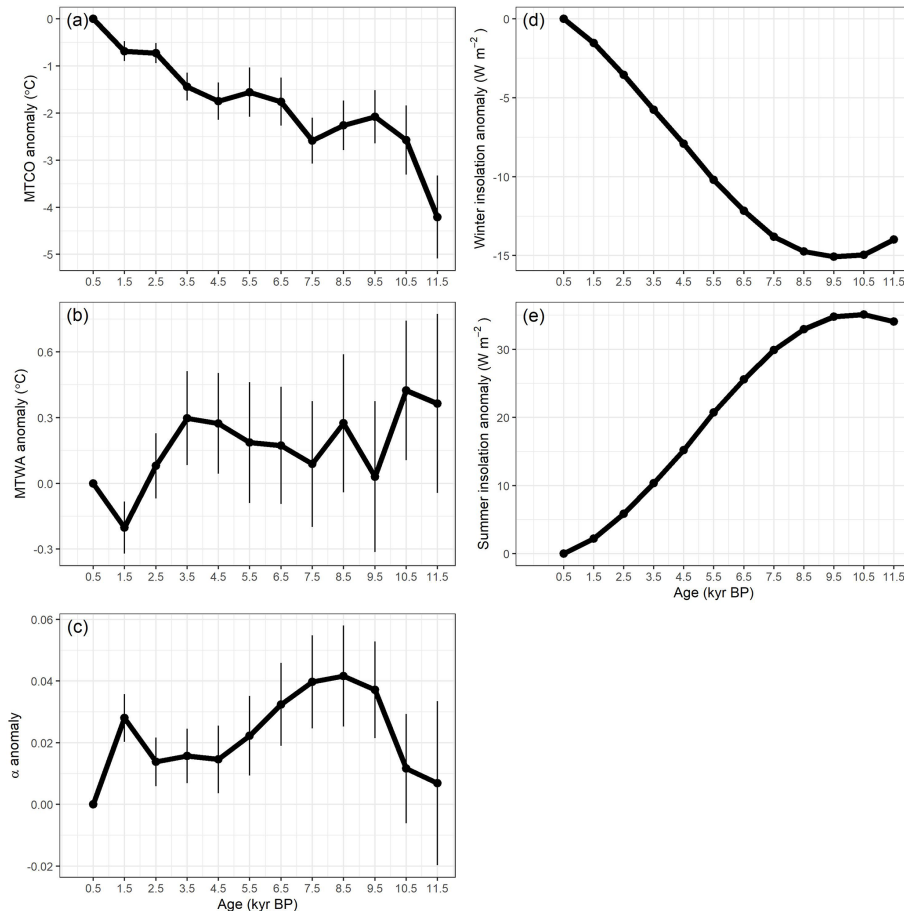


**Figure 4.** Reconstructed composite changes (anomalies to 0.5 ka) in **(a)** mean temperature of the coldest month (MTCO), **(b)** mean temperature of the warmest month (MTWA) and **(c)** plant-available moisture as represented by  $\alpha$ , through the Holocene compared to changes in **(d)** winter and **(e)** summer insolation for the latitude of the Iberian Peninsula, using  $\pm 500$  years as the bin. The black lines show mean values across sites, with vertical line segments showing the standard deviations of mean values using 1000 bootstrap cycles of site resampling.

increase in temperature from the Younger Dryas onwards, although the trend is less marked in the west than in the east (Baldini et al., 2019). This warming trend is consistent with our reconstructions of changes in MTCO through the Holocene. Speleothem records also show distinctly different patterns in moisture availability, with sites in western Iberia indicating wetter environments during the early Holocene and a transition to drier conditions from ca. 7.5 calkaBP to the present (Stoll et al., 2013; Thatcher et al., 2020), while eastern sites record wetter conditions persisting from 9 to 4 calka (Walczak et al., 2015). This finding would support the weaker west to east moisture gradient shown by our results.

Pollen data are widely used for the quantitative reconstruction of past climates (see discussion in Bartlein et al., 2011), but reconstructions of moisture indices are also affected by changes in water-use efficiency caused by the impact of changing atmospheric  $\text{CO}_2$  levels on plant physiology (Farquhar, 1997; Gerhart and Ward, 2010; Prentice et al.,

2017; Prentice and Harrison, 2009). This has been shown to be important on glacial–interglacial timescales, when intervals of lower-than-present  $\text{CO}_2$  result in vegetation appearing to reflect drier conditions than were experienced in reality (Prentice et al., 2011, 2017; Wei et al., 2021). We do not account for this  $\text{CO}_2$  effect in our reconstructions of  $\alpha$  because the change in  $\text{CO}_2$  over the Holocene was only 40 ppm. This change, relative to modern levels, only has a small impact on the reconstructions (Prentice et al., 2022) and is sufficiently small to be within the reconstruction uncertainties. Furthermore, accounting for changes in  $\text{CO}_2$  would not affect the reconstructed west–east gradient through time.

A more serious issue for our reconstructions may be the extent to which the vegetation cover of Iberia was substantially modified by human activities during the Holocene. Archaeological evidence shows that the introduction of agriculture during the Neolithic transition occurred ca. 7.6 ka in some southern and eastern areas of the Iberian Peninsula but spread slowly, and farming first occurred only around 6 ka in



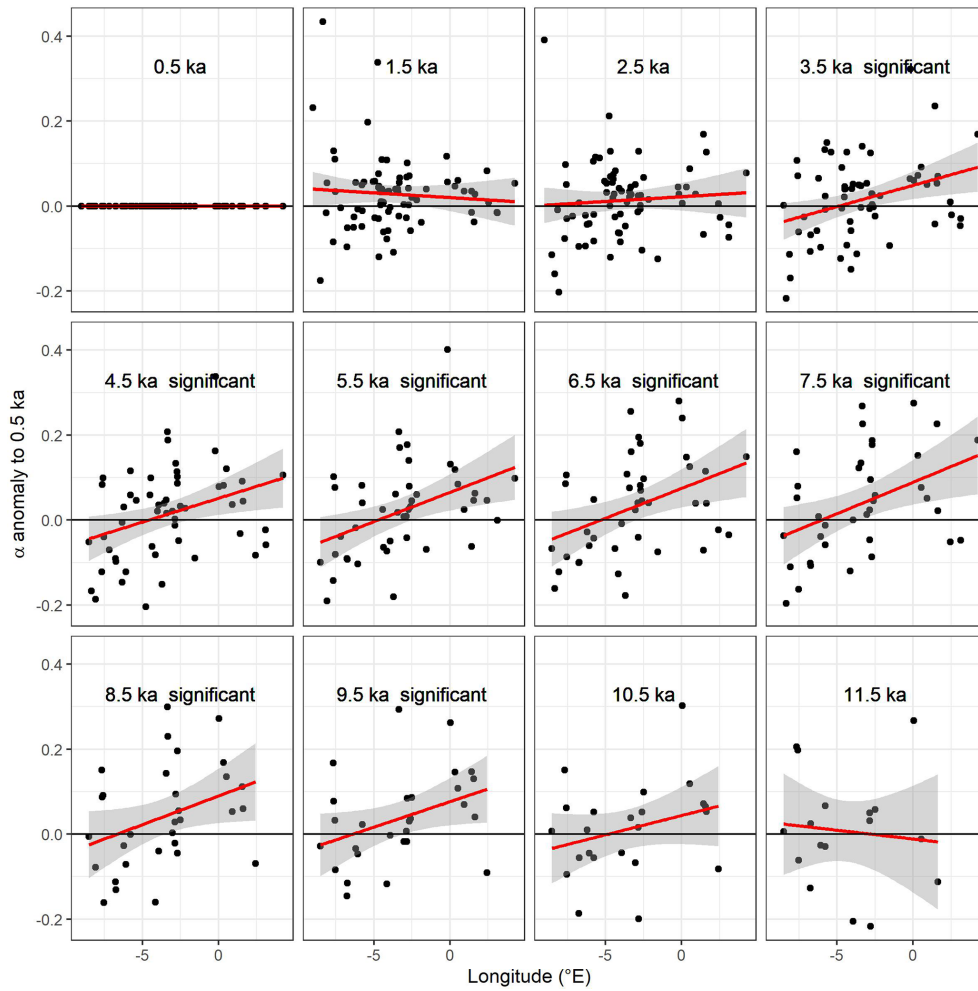


**Figure 5.** Changes in the west–east gradient of plant-available moisture as represented by anomalies in  $\alpha$  relative to 0.5 ka at individual sites through the Holocene. The red lines show the regression lines. The shades indicate the 95 % confidence intervals of the regression lines

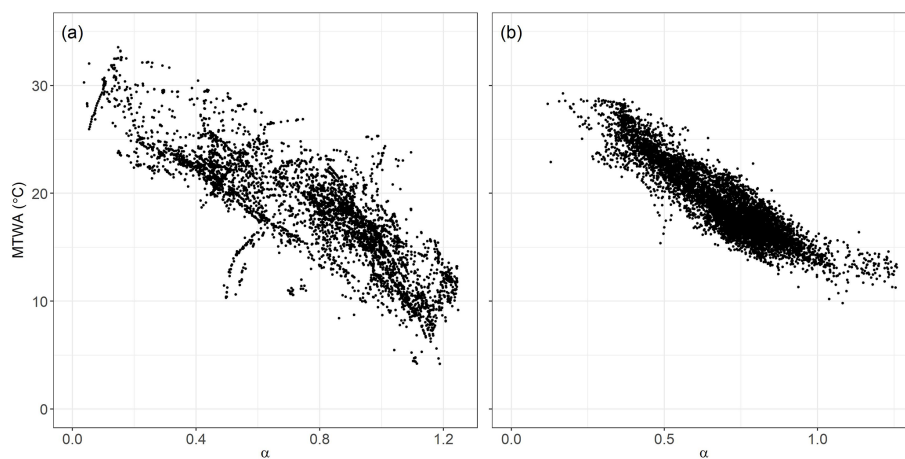


**Figure 6.** The relationship between mean temperature of the warmest month (MTWA) and plant-available moisture as represented by  $\alpha$  (a) in the modern climate data set and (b) in the Holocene reconstructions.

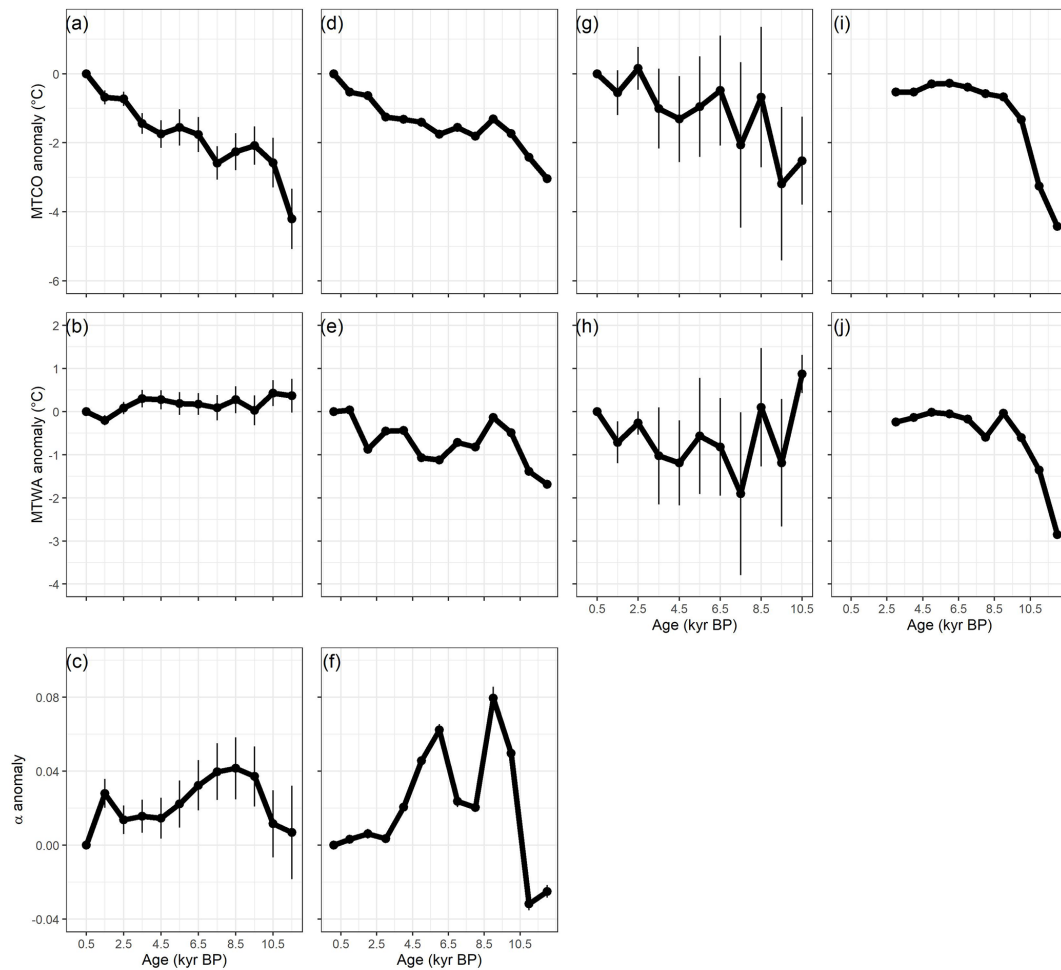


**Figure 7.** Comparison between reconstructed composite changes in climate anomalies. The first column represents this paper, the second column represents Mauri et al. (2015), the third column represents Kaufman et al. (2020) and the fourth column represents Tarroso et al. (2016). The composite curves from this paper and Kaufman et al. (2020) are calculated from individual reconstructions, using anomalies to 0.5 ka and a bin of  $\pm 500$  years (time slices are 0.5, 1.5, ..., 11.5 ka). The composite curves from Mauri et al. (2015) are converted directly from the gridded time slices which are provided with anomalies to 0.1 ka and a bin of  $\pm 500$  years (time slices are 1, 2, ..., 12 ka). The composite curves from Tarroso et al. (2016) are also converted directly from the gridded time slices provided, with anomalies to 0.5 ka and a bin of  $\pm 500$  years (time slices are 3, 4, ..., 12 ka). Note that Tarroso et al. (2016) applied a smoothing to the data such that the plots in their paper do not show the excursion in MTWA at 8 ka. In all of the plots, the black lines show mean values across sites, with vertical line bars showing the standard deviation of mean values using 1000 bootstrap cycles of site/grid resampling.

the northwest (Drake et al., 2017; Fyfe et al., 2019; Zapata et al., 2004). Anthropogenic changes in land use have been detected at a number of sites, based on pollen evidence of increases in weeds, the presence of cereals (e.g. Abel-Schaad and López-Sáez, 2013; Cortés Sánchez et al., 2012; López-Merino et al., 2010; Mighall et al., 2006; Peña-Chocarro et al., 2005) or the presence of fungal spores associated with animal faeces which has been used to identify the presence of domesticated animals (e.g. López-Sáez and López-Merino, 2007; Revelles et al., 2018). The presence of cereals is the most reliable source of data on human activities, but most cereals only release pollen during threshing and thus are not found in abundance in pollen diagrams from natural (as op-

posed to archaeological) sites (Trondman et al., 2015). Indeed, it is only after ca. 1 ka that the number of sites which record cereal pollen exceeds the number of sites at which cereals are not represented (Githumbi et al., 2022). Thus, while anthropogenic activities may have been important at the local scale and particularly in the later Holocene (e.g. Connor et al., 2019; Fyfe et al., 2019; Githumbi et al., 2022), most of the sites used for our reconstructions are not associated with archaeological evidence of agriculture or substantial landscape modification. Furthermore, the consistency of the reconstructed changes in climate across sites provides support for these being largely a reflection of regional climate changes rather than human activities.

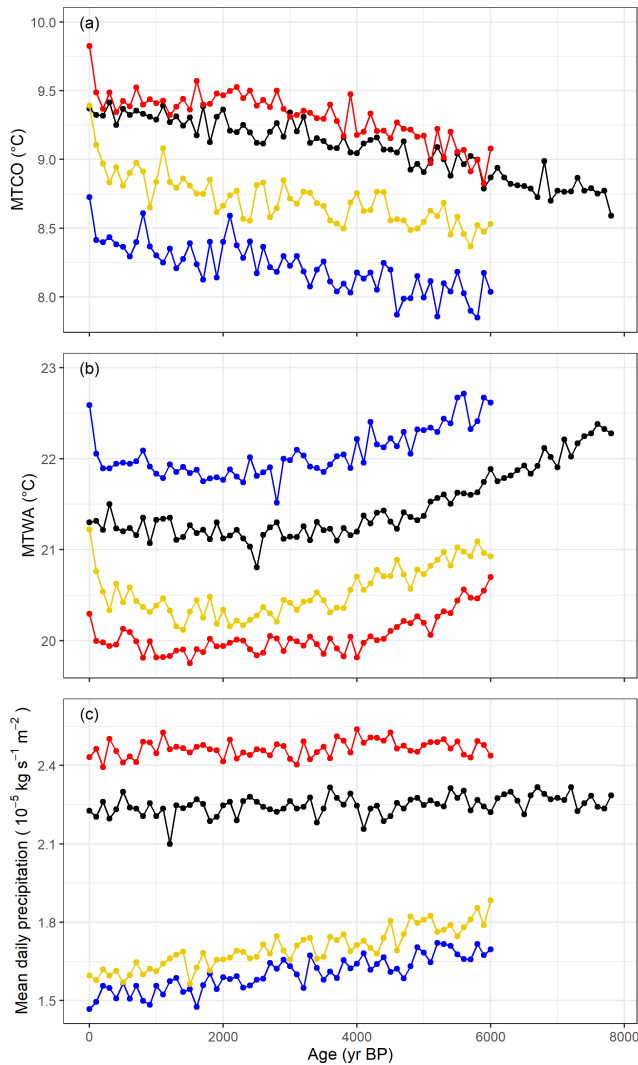


**Figure 8.** Simulated mean values of mean temperature of the coldest month (MTCO), mean temperature of the warmest month (MTWA) and mean daily precipitation in the Iberian Peninsula between 8 and 0 ka, smoothed using 100-year bins. Here, BP means before 1950 AD. The black lines represent the Max Planck Institute (MPI) Earth system model simulations, the red lines represent the Alfred Wagner Institute (AWI) Earth system model simulations, the blue lines represent the Institut Pierre-Simon Laplace Climate Model (IPSL-CM5) TR5AS simulations and the gold lines represent the Institut Pierre-Simon Laplace Climate Model (IPSL-CM6) TR6AV simulations. The four simulations were forced by evolving orbital parameters and greenhouse gas concentrations. The four models have different spatial resolutions, with the finest resolution being  $1.875^\circ \times 1.875^\circ$  (AWI, MPI) and the coarsest resolution being  $1.875^\circ \times 3.75^\circ$  (IPSL-CM5, TR5AS).

We have used a modified version of fxTWA-PLS to reconstruct Holocene climates of the Iberian Peninsula because this modification reduced the compression bias in MTCO and MTWA, and specifically reduces the maximum bias in MTCO, MTWA and  $\alpha$ . Although this modified approach produces better overall reconstructions (Appendix A), its use does not change the reconstructed trends in these variables through time (Fig. S10). Thus, the finding that winter temperatures are a direct reflection of insolation forcing while summer temperatures are influenced by land-surface feedbacks and changes in atmospheric circulation is robust to the version of fxTWA-PLS used. However, while we use a much larger data set than previous reconstructions, the distribution of pollen sites is uneven and the northern part of the Peninsula is better sampled than the southwest, which could lead to some uncertainties in the interpretation of changes in the west–east gradient of moisture. It would therefore be useful to specifically target the southwestern part of the Iberian Peninsula for new data collection. Alternatively, it would be useful to apply the approach used here to the whole of Eurasia, given that the failure of state-of-the-art climate models to advect moisture into the continental interior appears to be a feature of the whole region (Bartlein et al., 2017) and not the peninsula alone.

## 5 Conclusion

We have developed an improved version of fxTWA-PLS which further reduces compression bias and provides robust climate reconstructions. We have used this technique with a large pollen data set representing 117 sites across the Iberian Peninsula to make quantitative reconstructions of summer and winter temperature and an index of plant-available moisture through the Holocene. We show that there was a gradual increase in winter temperature through the Holocene and that this trend broadly follows the changes in orbital forcing. Summer temperatures, however, do not follow the changes in orbital forcing but appear to be influenced by land-surface feedbacks associated with changes in moisture. We show that the west–east gradient in moisture was considerably less pronounced during the mid-Holocene, implying a significant increase in moisture advection into the continental interior resulting from changes in circulation. Our reconstructions of temperature changes are broadly consistent with previous reconstructions but are more solidly based because of the increased site coverage. Our reconstructions of changes in the west–east gradient of moisture during the early part of the Holocene are also consistent with previous reconstructions, although this change is not simulated by state-of-the-art climate models, implying that there are still issues with resolving the associated land-surface feedbacks in these models. Our work provides an improved foundation for documenting and understanding the Holocene palaeoclimates of Iberia.

**Appendix A: Theoretical basis**

**The previous version of fxTWA-PLS (fxTWA-PLS1)**

The estimated optimum ( $\hat{u}_k$ ) and unbiased tolerance ( $\hat{t}_k$ ) of each taxon are calculated from the modern training data set as follows:

$$\hat{u}_k = \frac{\sum_{i=1}^n y_{ik} x_i}{\sum_{i=1}^n y_{ik}}, \tag{A1}$$

$$\hat{t}_k = \sqrt{\frac{\sum_{i=1}^n y_{ik} (x_i - \hat{u}_k)^2}{(1 - 1/N_{2k}) \sum_{i=1}^n y_{ik}}}, \tag{A2}$$

where

$$N_{2k} = \frac{1}{\sum_{i=1}^n \left( \frac{y_{ik}}{\sum_{i'=1}^n y_{i'k}} \right)^2}, \tag{A3}$$

where  $n$  is the total number of sites;  $y_{ik}$  is the observed abundance of the  $k$ th taxon at the  $i$ th site;  $x_i$  is the observed climate value at the  $i$ th site and  $N_{2k}$  is the effective number of occurrences for the  $k$ th taxon.

The fx correction is applied as weight in the form of  $1/\text{fx}^2$  at regression at step 7 in Table 1 in Liu et al. (2020). The regression step uses robust linear model fitting by the R code:

$$\text{rlm} \left( x_i \sim \text{comp}_1 + \text{comp}_2 + \dots + \text{comp}_{\text{pls}}, \text{weights} = 1/\text{fx}^2 \right). \tag{A4}$$

**The modified version of fxTWA-PLS (fxTWA-PLS2)**

The distribution of  $y_{ik}$  is influenced by the distribution of the climate variable, so we need to apply the fx correction when calculating optimum and tolerance for each taxon as follows:

$$\hat{u}_k = \frac{\sum_{i=1}^n \frac{y_{ik} x_i}{f_{x_i}}}{\sum_{i=1}^n \frac{y_{ik}}{f_{x_i}}}, \tag{A5}$$

$$\hat{t}_k = \sqrt{\frac{\sum_{i=1}^n \frac{y_{ik} (x_i - \hat{u}_k)^2}{f_{x_i}}}{\left(1 - \frac{1}{N_{2k}}\right) \sum_{i=1}^n \frac{y_{ik}}{f_{x_i}}}}, \tag{A6}$$

where

$$N_{2k} = \frac{1}{\sum_{i=1}^n \left( \frac{\frac{y_{ik}}{f_{x_i}}}{\sum_{i'=1}^n \frac{y_{i'k}}{f_{x_{i'}}}} \right)^2}. \tag{A7}$$

The modified version of fxTWA-PLS applies fx correction separately at taxon calculation and regression (step 2 and step 7 in Table 1 in Liu et al., 2020), both using weight in the form of  $1/\text{fx}$ . The regression step (step 7) then becomes

$$\text{rlm} \left( x_i \sim \text{comp}_1 + \text{comp}_2 + \dots + \text{comp}_{\text{pls}}, \text{weights} = 1/\text{fx} \right). \tag{A8}$$

The previous version uses fx values extracted from histograms, and different bin widths may result in different training results. The modified version applies P-splines histogram smoothing (Eilers and Marx, 2021) with third-order difference penalty, which makes the fx values almost independent of the bin width. The optimal smoothing parameter of the P-splines penalty was determined by the HFS (Harville–Fellner–Schall) algorithm (Eilers and Marx, 2021) for the Poisson likelihood for the histogram counts.

**Table A1.** Leave-out cross-validation (with geographically and climatically close sites removed) fitness of the previous and modified version of fxTWA-PLS (fxTWA-PLS1 and fxTWA-PLS2, respectively), for the mean temperature of the coldest month (MTCO), mean temperature of the warmest month (MTWA) and plant-available moisture ( $\alpha$ ), using bins of 0.02, 0.02 and 0.002, respectively;  $n$  is the number of components used; Avg.bias is the average bias, while Max.bias is the maximum absolute bias and Min.bias is the minimum absolute bias; RMSEP is the root mean square error of prediction; and  $\Delta$ RMSEP is the per cent change rate of RMSEP, which is  $(RMSEP_n - RMSEP_{n-1})/RMSEP_{n-1}$  converted into percentage; when  $n = 1$ ,  $RMSEP_0$  is the RMSEP of null model.  $p$  assesses whether using the current number of components is significantly different from using one component less, which is used to choose the last significant number of components (indicated in bold) to avoid overfitting. The degree of overall compression is assessed by doing linear regression to the cross-validation result and the climate variable;  $b_1$  and  $b_1.se$  are the slope and the standard error of the slope, respectively. The closer the slope ( $b_1$ ) is to 1, the lower the overall compression is. The fx correction is set intrinsically in functions of the fxTWA-PLS package for both versions in this paper, instead of relying on an outside input in Liu et al. (2020), so the values of fxTWA-PLS1 might be slightly different from values in Table 3 of Liu et al. (2020), but it does not affect the conclusion.

	Method	$n$	$R^2$	Avg. bias	Max. bias	Min. bias	RMSEP	$\Delta$ RMSEP	$p$	$b_1$	$b_1.se$
MTCO	fxTWA-PLS1	1	0.66	-0.86	31.17	0.00	5.21	-39.87	0.001	0.76	0.01
		2	0.72	-0.52	36.65	0.00	4.70	-9.78	0.001	0.80	0.01
		3	0.73	-0.47	41.18	0.00	4.62	-1.63	0.001	0.82	0.01
		<b>4</b>	<b>0.73</b>	<b>-0.51</b>	<b>44.86</b>	<b>0.00</b>	<b>4.58</b>	<b>-1.01</b>	<b>0.006</b>	<b>0.82</b>	<b>0.01</b>
		5	0.73	-0.41	58.35	0.00	4.62	0.89	0.708	0.83	0.01
	fxTWA-PLS2	1	0.70	-0.86	25.23	0.00	5.20	-39.97	0.001	0.89	0.01
		2	0.73	-0.73	25.00	0.00	4.87	-6.29	0.001	0.91	0.01
		3	0.74	-0.71	24.38	0.00	4.86	-0.32	0.001	0.91	0.01
		<b>4</b>	<b>0.75</b>	<b>-0.59</b>	<b>24.27</b>	<b>0.00</b>	<b>4.70</b>	<b>-3.26</b>	<b>0.001</b>	<b>0.91</b>	<b>0.01</b>
		5	0.74	-0.63	34.54	0.00	4.77	1.51	1.000	0.91	0.01
MTWA	fxTWA-PLS1	1	0.50	-0.53	17.91	0.00	3.87	-24.09	0.001	0.67	0.01
		<b>2</b>	<b>0.56</b>	<b>-0.54</b>	<b>17.71</b>	<b>0.00</b>	<b>3.52</b>	<b>-8.98</b>	<b>0.001</b>	<b>0.69</b>	<b>0.01</b>
		3	0.57	-0.49	25.14	0.00	3.52	0.09	0.565	0.73	0.01
		4	0.57	-0.43	34.92	0.00	3.56	1.12	0.974	0.75	0.01
		5	0.57	-0.46	32.23	0.00	3.55	-0.23	0.139	0.74	0.01
	fxTWA-PLS2	1	0.52	-0.29	17.13	0.00	3.72	-26.88	0.001	0.69	0.01
		2	0.56	-0.14	17.20	0.00	3.53	-5.06	0.001	0.71	0.01
		3	0.56	-0.13	17.01	0.00	3.53	-0.20	0.008	0.71	0.01
		<b>4</b>	<b>0.57</b>	<b>-0.11</b>	<b>17.30</b>	<b>0.00</b>	<b>3.47</b>	<b>-1.56</b>	<b>0.001</b>	<b>0.71</b>	<b>0.01</b>
		5	0.57	-0.11	17.34	0.00	3.48	0.10	0.780	0.71	0.01
$\alpha$	fxTWA-PLS1	1	0.63	-0.020	0.773	0.000	0.174	-36.23	0.001	0.78	0.01
		2	0.69	-0.012	0.902	0.000	0.157	-9.66	0.001	0.79	0.01
		<b>3</b>	<b>0.69</b>	<b>-0.011</b>	<b>0.820</b>	<b>0.000</b>	<b>0.155</b>	<b>-1.28</b>	<b>0.001</b>	<b>0.79</b>	<b>0.01</b>
		4	0.70	-0.010	0.786	0.000	0.156	0.25	0.867	0.81	0.01
		5	0.70	-0.010	0.786	0.000	0.156	0.09	1.000	0.81	0.01
	fxTWA-PLS2	1	0.65	-0.014	0.787	0.000	0.165	-39.59	0.001	0.76	0.01
		2	0.68	-0.016	0.781	0.000	0.159	-3.55	0.001	0.77	0.01
		<b>3</b>	<b>0.68</b>	<b>-0.017</b>	<b>0.757</b>	<b>0.000</b>	<b>0.158</b>	<b>-0.61</b>	<b>0.023</b>	<b>0.78</b>	<b>0.01</b>
		4	0.69	-0.017	0.784	0.000	0.158	-0.43	0.108	0.79	0.01
		5	0.69	-0.017	0.850	0.000	0.158	0.26	0.985	0.80	0.01

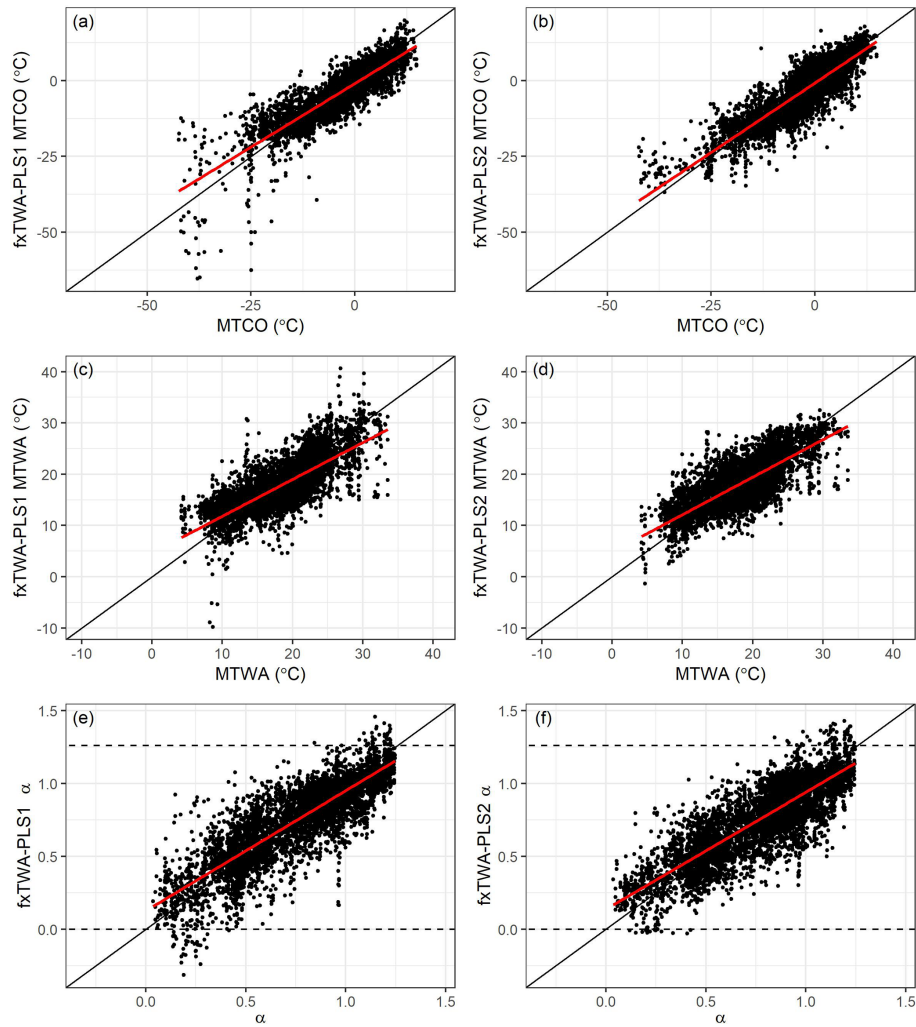


**Figure A1.** Training result using the last significant number of components for mean temperature of the coldest month (MTCO), mean temperature of the warmest month (MTWA) and plant-available moisture ( $\alpha$ ). The left column (a, c and e) shows the previous version (fXTWA-PLS1) and the right column (b, d and f) shows the modified version of fXTWA-PLS (fXTWA-PLS2). The 1 : 1 line is shown in black; the linear regression line is shown in red to show the degree of overall compression. The horizontal dashed lines indicate the natural limit of  $\alpha$  (0–1.26).

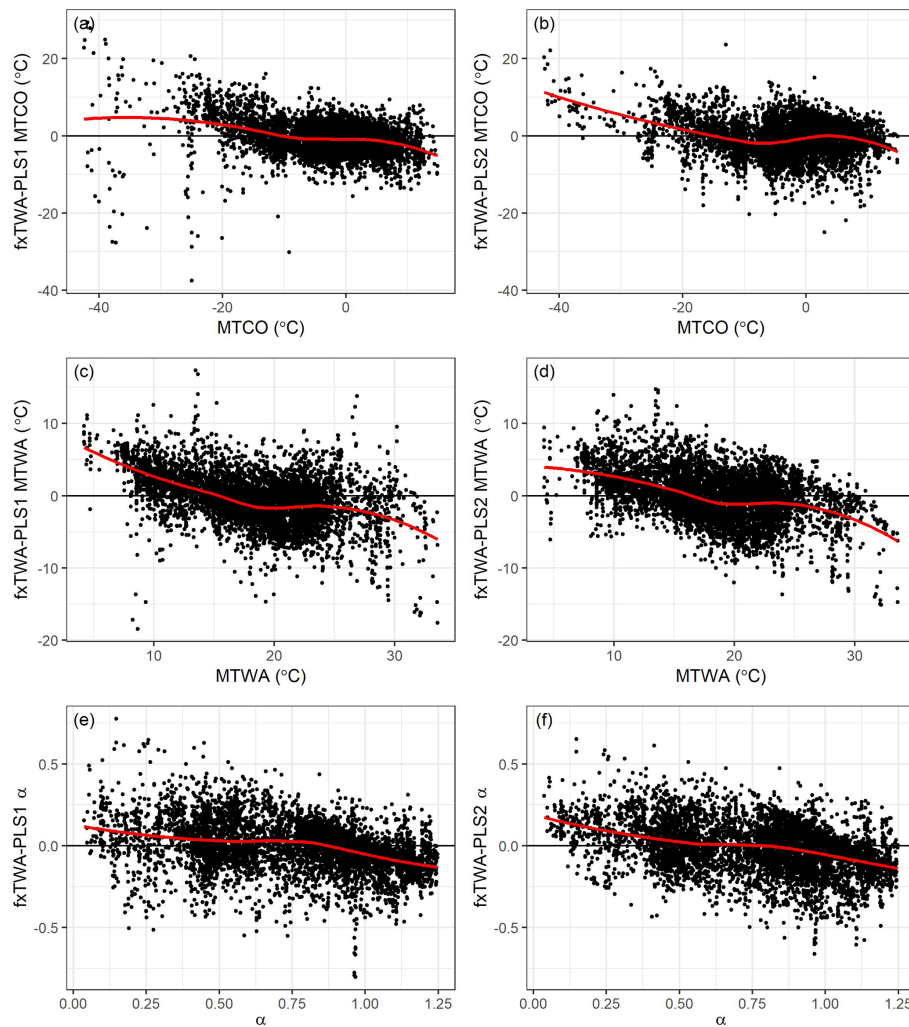


**Figure A2.** Residual using the last significant number of components for mean temperature of the coldest month (MTCO), mean temperature of the warmest month (MTWA) and plant-available moisture ( $\alpha$ ). The left column (a, c and e) shows the previous version (fxTWA-PLS1) and the right column (b, d and f) shows the modified version (fxTWA-PLS2) of fxTWA-PLS. The zero line is shown in black; the locally estimated scatterplot smoothing is shown in red to show the degree of local compression.

**Code and data availability.** All the data used are public access and cited here. The code used to generate the climate reconstructions is available at <https://doi.org/10.5281/zenodo.7714294> (Liu, 2023).

**Supplement.** The supplement related to this article is available online at: <https://doi.org/10.5194/cp-19-803-2023-supplement>.

**Author contributions.** ML, ICP and SPH designed the study. ML, ICP and CJFtB gave insights into the regional palaeoclimate histories. ML carried out the analyses. ML and SPH wrote the first draft of the paper and all authors contributed to the final draft.

**Competing interests.** The contact author has declared that none of the authors has any competing interests.

**Disclaimer.** Publisher's note: Copernicus Publications remains neutral with regard to jurisdictional claims in published maps and institutional affiliations.

**Acknowledgements.** Mengmeng Liu acknowledges support from Imperial College through the Lee Family Scholarship. Yicheng Shen and Sandy P. Harrison acknowledge support from the ERC-funded project GC 2.0 (“Global Change 2.0: Unlocking the past for a clearer future”; grant number 694481). Iain Colin Prentice acknowledges support from the ERC under the European Union Horizon 2020 research and innovation programme (grant

agreement no.: 787203 REALM). This work is a contribution to the project “Origen y Cuantificación de los Cambios Paleoclimáticos en el Pirineo: Variabilidad climática e impacto humano” (PYCACHU: PID2019-106050RB-I00) funded by the Ministerio de Ciencia e Innovación.

**Financial support.** This research has been supported by the Lee Family Scholarship fund, the European Research Council (GC2.0, grant no. 694481 and REALM, grant no. 787203) and the Ministerio de Ciencia e Innovación (PYCACHU, grant no. PID2019-106050RB-I00).

**Review statement.** This paper was edited by Nathalie Combourieu Nebout and reviewed by four anonymous referees.

## References

- Abel-Schaad, D. and López-Sáez, J. A.: Vegetation changes in relation to fire history and human activities at the Peña Negra mire (Bejar Range, Iberian Central Mountain System, Spain) during the past 4,000 years, *Veg. Hist. Archaeobot.*, 22, 199–214, <https://doi.org/10.1007/s00334-012-0368-9>, 2013.
- Abel-Schaad, D., Hernández-Carretero, A. M., López-Merino, L., Pulido-Díaz, F. J., and López-Sáez, J. A.: Cabras y quemorros: tres siglos de cambios en el paisaje de la vertiente extremeña de la Sierra de Gredos, *Rev. Estud. Extremeños*, 65, 449–478, 2009a.
- Abel-Schaad, D., Hernández, A., López-Sáez, J. A., Pulido-Díaz, F. J., López-Merino, L., and Martínez-Cortizas, A.: Evolución de la vegetación en la Sierra de Gata (Cáceres–Salamanca, España) durante el Holoceno reciente. Implicaciones biogeográficas, *Rev. Española Micropaleontol.*, 41, 91–105, 2009b.
- Abel-Schaad, D., Alba-Sánchez, F., Pérez-Díaz, S., and López-Sáez, J. A.: 36. Praillos de Boissier mire, Tejada Natural Park (Baetic Range, southern Spain), *Grana*, 56, 475–477, 2017.
- Alba-Sánchez, F., López-Sáez, J. A., Abel-Schaad, D., Sabariego-Ruiz, S., Pérez-Díaz, S., González-Hernández, A., and Linares, J. C.: The impact of climate and land-use changes on the most southerly fir forests (*Abies pinsapo*) in Europe, *The Holocene*, 29, 1176–1188, 2019.
- Allen, J. R. M., Huntley, B., and Watts, W. A.: The vegetation and climate of northwest Iberia over the last 14,000 years, *J. Quaternary Sci.*, 11, 125–147, 1996.
- Allison, P. D.: *Multiple Regression: A Primer*, Pine Forge Press, ISBN 10:0761985336, ISBN 13:9780761985334, 1994.
- Anderson, R. S., Jiménez-Moreno, G., Carrión, J. S., and Pérez-Martínez, C.: Postglacial history of alpine vegetation, fire, and climate from Laguna de Río Seco, Sierra Nevada, southern Spain, *Quaternary Sci. Rev.*, 30, 1615–1629, 2011.
- Andrade, C., Contente, J., and Santos, J. A.: Climate change projections of aridity conditions in the Iberian Peninsula, *Water*, 13, 2035, <https://doi.org/10.3390/w13152035>, 2021a.
- Andrade, C., Contente, J., and Santos, J. A.: Climate change projections of dry and wet events in Iberia based on the WASP-Index, *Climate*, 9, 94, <https://doi.org/10.3390/cli9060094>, 2021b.
- Aranbarri, J., Gonzalez Samperiz, P., Valero-Garcés, B., Moreno, A., Gil-Romera, G., Sevilla-Callejo, M., Garcia-Prieto, E., Di Rita, F., Mata, M. P., Morellón, M., Magri, D., Rodríguez-Lázaro, J., and Carrión, J.: Rapid climatic changes and resilient vegetation during the Lateglacial and Holocene in a continental region of south-western Europe, *Global Planet. Change*, 114, 50–65, <https://doi.org/10.1016/j.gloplacha.2014.01.003>, 2014.
- Aranbarri, J., González-Sampériz, P., Iriarte, E., Moreno, A., Rojo-Guerra, M., Peña-Chocarro, L., Valero-Garcés, B., Leunda, M., García-Prieto, E., Sevilla-Callejo, M., Gil-Romera, G., Magri, D., and Rodríguez-Lázaro, J.: Human–landscape interactions in the Conquezueta–Ambrona Valley (Soria, continental Iberia): From the early Neolithic land use to the origin of the current oak woodland, *Palaeogeogr. Palaeoclimatol. Palaeoecol.*, 436, 41–57, <https://doi.org/10.1016/j.palaeo.2015.06.030>, 2015.
- Baldini, L. M., Baldini, J. U. L., McDermott, F., Arias, P., Cueto, M., Fairchild, I. J., Hoffmann, D. L., Matthey, D. P., Müller, W., Nita, D. C., Ontañón, R., García-Moncó, C., and Richards, D. A.: North Iberian temperature and rainfall seasonality over the Younger Dryas and Holocene, *Quaternary Sci. Rev.*, 226, 105998, <https://doi.org/10.1016/j.quascirev.2019.105998>, 2019.
- Bartlein, P. J., Prentice, I. C., and Webb, T.: Climatic response surfaces from pollen data for some Eastern North American taxa, *J. Biogeogr.*, 13, 35J. *Biogeogr.*, <https://doi.org/10.2307/2844848>, 1986.
- Bartlein, P. J., Harrison, S. P., Brewer, S., Connor, S., Davis, B. A. S., Gajewski, K., Guiot, J., Harrison-Prentice, T. I., Henderson, A., Peyron, O., Prentice, I. C., Scholze, M., Seppä, H., Shuman, B., Sugita, S., Thompson, R. S., Viau, A. E., Williams, J., and Wu, H.: Pollen-based continental climate reconstructions at 6 and 21 ka: A global synthesis, *Clim. Dynam.*, 37, 775–802, <https://doi.org/10.1007/s00382-010-0904-1>, 2011.
- Bartlein, P. J., Harrison, S. P., and Izumi, K.: Underlying causes of Eurasian midcontinental aridity in simulations of mid-Holocene climate, *Geophys. Res. Lett.*, 44, 9020–9028, <https://doi.org/10.1002/2017GL074476>, 2017.
- Blaauw, M. and Christeny, J. A.: Flexible paleoclimate age-depth models using an autoregressive gamma process, *Bayesian Anal.*, 6, 457–474, <https://doi.org/10.1214/11-BA618>, 2011.
- Blaauw, M., Christen, J. A., Aquino Lopez, M. A., Esquivel Vazquez, J., Gonzalez V., O. M., Belding, T., Theiler, J., Gough, B., and Karney, C.: rbacon: Age-depth modelling using Bayesian statistics, <https://cran.r-project.org/package=rbacon> (last access: 10 March 2023), 2021.
- Braconnot, P., Crétat, J., Marti, O., Balkanski, Y., Caubel, A., Cozic, A., Foujols, M.-A., and Sanogo, S.: Impact of multiscale variability on last 6,000 years Indian and West African monsoon rain, *Geophys. Res. Lett.*, 46, 14021–14029, <https://doi.org/10.1029/2019GL084797>, 2019.
- Brierley, C. M., Zhao, A., Harrison, S. P., Braconnot, P., Williams, C. J. R., Thornalley, D. J. R., Shi, X., Peterschmitt, J.-Y., Ohgaito, R., Kaufman, D. S., Kageyama, M., Hargreaves, J. C., Erb, M. P., Emile-Geay, J., D’Agostino, R., Chandan, D., Carré, M., Bartlein, P. J., Zheng, W., Zhang, Z., Zhang, Q., Yang, H., Volodin, E. M., Tomas, R. A., Routson, C., Peltier, W. R., Otto-Bliesner, B., Morozova, P. A., McKay, N. P., Lohmann, G., Legrande, A. N., Guo, C., Cao, J., Brady, E., Annan, J. D., and Abe-Ouchi, A.: Large-scale features and evaluation of the



- PMIP4-CMIP6 *midHolocene* simulations, *Clim. Past*, 16, 1847–1872, <https://doi.org/10.5194/cp-16-1847-2020>, 2020.
- Burjachs, F.: Palynology of the Upper Pleistocene and Holocene of the north-east Iberian Peninsula: Pla De L'Estany (Catalonia), *Hist. Biol.*, 9, 17–33, 1994.
- Burjachs, F.: La secuencia palinológica de La Cruz (Cuenca, España), in *Estudios Palinológicos*, edited by: Ruz-Zapata, M. B., Publicaciones de la Universidad de Alcalá, 31–36, ISBN 84-8138-168-3, 1996.
- Burjachs, F. and Expósito, I.: Charcoal and pollen analysis: Examples of Holocene fire dynamics in Mediterranean Iberian Peninsula, *Catena*, 135, 340–349, 2015.
- Burjachs, F., Pérez-Obiol, R., Roure, J. M. and Julià, R.: Dinámica de la vegetación durante el Holoceno en la isla de Mallorca, in *Trabajos de Palinología básica y aplicada*, edited by: Mateu, I., Dupré, M., Güemes, J., and Burgaz, M. E., Universitat de València, València, 199–210, ISBN 84-370-1637-1, 1994.
- Burjachs, F., Giralt, S., Roca, J. R., Seret, G., and Julia, R.: Palinología holocénica y desertización en el mediterráneo occidental, in *El paisaje mediterráneo a través del espacio y del tiempo. Implicaciones en la desertización*, edited by: Ibáñez, J. J., Valero Garcés, B. L., and Machado, C., Geoforma Ediciones, 379–394, ISBN 84-87779-30-1, 1997.
- Burjachs, F., Pérez-Obiol, R., Picornell-Gelabert, L., Revelles, J., Servera-Vives, G., Expósito, I., and Yll, E. I.: Overview of environmental changes and human colonization in the Balearic Islands (Western Mediterranean) and their impacts on vegetation composition during the Holocene, *J. Archaeol. Sci. Reports*, 12, 845–859, <https://doi.org/10.1016/j.jasrep.2016.09.018>, 2017.
- Camarero, J. J., Sangüesa-Barreda, G., Pérez-Díaz, S., Montiel-Molina, C., Seijo, F., and López-Sáez, J. A.: Abrupt regime shifts in post-fire resilience of Mediterranean mountain pinewoods are fuelled by land use, *Int. J. Wildl. Fire*, 28, 329–341, <https://doi.org/10.1071/WF18160>, 2019.
- Camuera, J., Ramos-Román, M. J., Jiménez-Moreno, G., García-Alix, A., Ilvonen, L., Ruha, L., Gil-Romera, G., González-Sampérez, P., and Seppä, H.: Past 200 kyr hydroclimate variability in the western Mediterranean and its connection to the African Humid Periods, *Sci. Rep.-UK*, 12, 9050, <https://doi.org/10.1038/s41598-022-12047-1>, 2022.
- Cano Villanueva, J. P.: Estudi palinologic de sediments litorals de la provincia d'Imeria. Transformacions del paisatge vegetal en un territori semiarid, Universitat Autònoma de Barcelona, Barcelona, Spain, 1997.
- Carré, M., Braconnot, P., Elliot, M., d'Agostino, R., Schurer, A., Shi, X., Marti, O., Lohmann, G., Jungclaus, J., Cheddadi, R., di Carlo, I. A., Cardich, J., Ochoa, D., Salas Gismondi, R., Pérez, A., Romero, P. E., Turcq, B., Corrège, T., and Harrison, S. P.: High-resolution marine data and transient simulations support orbital forcing of ENSO amplitude since the mid-Holocene, *Quaternary Sci. Rev.*, 268, 107125, <https://doi.org/10.1016/j.quascirev.2021.107125>, 2021.
- Carrión, J. S.: Patterns and processes of Late Quaternary environmental change in a montane region of southwestern Europe, *Quaternary Sci. Rev.*, 21, 2047–2066, 2002.
- Carrión, J. S. and Dupré, M.: Late Quaternary vegetational history at Navarrés, Eastern Spain. A two core approach, *New Phytol.*, 134, 177–191, 1996.
- Carrión, J. S. and van Geel, B.: Fine-resolution Upper Weichselian and Holocene palynological record from Navarrés (Valencia, Spain) and a discussion about factors of Mediterranean forest succession, *Rev. Palaeobot. Palynol.*, 106, 209–236, [https://doi.org/10.1016/S0034-6667\(99\)00009-3](https://doi.org/10.1016/S0034-6667(99)00009-3), 1999.
- Carrión, J. S., Munuera, M., Dupré, M., and Andrade, A.: Abrupt vegetation changes in the Segura Mountains of southern Spain throughout the Holocene, *J. Ecol.*, 89, 783–797, <https://doi.org/10.1046/j.0022-0477.2001.00601.x>, 2001a.
- Carrión, J. S., Andrade, A., Bennett, K. D., Navarro, C., and Munuera, M.: Crossing forest thresholds: Inertia and collapse in a Holocene sequence from south-central Spain, *The Holocene*, 11, 635–653, <https://doi.org/10.1191/09596830195672>, 2001b.
- Carrión, J. S., Sánchez-Gómez, P., Mota, J. F., Yll, R., and Chaín, C.: Holocene vegetation dynamics, fire and grazing in the Sierra de Gádor, southern Spain, *The Holocene*, 13, 839–849, 2003.
- Carrión, J. S., Yll, E. I., Willis, K. J., and Sánchez, P.: Holocene forest history of the eastern plateaux in the Segura Mountains (Murcia, southeastern Spain), *Rev. Palaeobot. Palynol.*, 132, 219–236, 2004.
- Carrión, J. S., Fuentes, N., González-Sampérez, P., Sánchez-Quirante, L., Finlayson, J. C., Fernández, S., and Andrade, A.: Holocene environmental change in a montane region of southern Europe with a long history of human settlement, *Quaternary Sci. Rev.*, 26, 1455–1475, <https://doi.org/10.1016/j.quascirev.2007.03.013>, 2007.
- Carrión, J. S., Fernández, S., González-Sampérez, P., Gil-Romera, G., Badal, E., Carrión-Marco, Y., López-Merino, L., López-Sáez, J. A., Fierro, E., and Burjachs, F.: Expected trends and surprises in the Lateglacial and Holocene vegetation history of the Iberian Peninsula and Balearic Islands, *Rev. Palaeobot. Palynol.*, 162, 458–475, <https://doi.org/10.1016/j.revpalbo.2009.12.007>, 2010.
- Carrión, Y., Kaal, J., López-Sáez, J. A., López-Merino, L., and Martínez Cortizas, A.: Holocene vegetation changes in NW Iberia revealed by anthracological and palynological records from a colluvial soil, *The Holocene*, 20, 53–66, <https://doi.org/10.1177/0959683609348849>, 2009.
- Carvalho, D., Pereira, S., and Rocha, A.: Future surface temperature changes for the Iberian Peninsula according to EURO-CORDEX climate projections, *Clim. Dynam.*, 56, 1–16, <https://doi.org/10.1007/s00382-020-05472-3>, 2021.
- Cerrillo-Cuenca, E. and González-Cordero, A.: Burial prehistoric caves in the interior basin of River Tagus: The complex at Canaleja Gorge (Romangordo, Cáceres, Spain), in: *From the origins: the Prehistory of Inner Tagus Region*. British Archaeological Reports 2219, vol. 2219, edited by: Bueno Ramírez, P., Cerrillo Cuenca, E., and González Cordero, A., Publishers of British Archaeological Reports, 21–42, <http://hdl.handle.net/10261/239930> (last access: 10 March 2023), 2011.
- Cerrillo-Cuenca, E., González-Cordero, A. and López-Sáez, J. A.: El proyecto de investigación de Garganta Canaleja: aproximación al análisis del Epipaleolítico y el Neolítico en el valle interior del Tajo, *Los Prim, Campesinos la Raya*, 6, 13–27, <http://hdl.handle.net/10261/137932> (last access: 10 March 2023), 2007.
- Cheddadi, R., Yu, G., Guiot, J., Harrison, S. P., and Prentice, I. C.: The climate of Europe 6000 years ago, *Clim. Dynam.*, 13, 1, <https://doi.org/10.1007/s003820050148>, 1997.

- Chevalier, M., Davis, B. A. S., Heiri, O., Seppä, H., Chase, B. M., Gajewski, K., Lacourse, T., Telford, R. J., Finsinger, W., Guiot, J., Kühl, N., Maezumi, S. Y., Tipton, J. R., Carter, V. A., Brussel, T., Phelps, L. N., Dawson, A., Zanon, M., Vallé, F., Nolan, C., Mauri, A., de Vernal, A., Izumi, K., Holmström, L., Marsicek, J., Goring, S., Sommer, P. S., Chaput, M., and Kupriyanov, D.: Pollen-based climate reconstruction techniques for late Quaternary studies, *Earth-Sci. Rev.*, 210, 103384, <https://doi.org/10.1016/j.earscirev.2020.103384>, 2020.
- Connor, S., Vanni re, B., Colombaroli, D., Anderson, R., Carri n, J., Ejarque, A., Gil-Romera, G., Gonzalez Samperiz, P., H fer, D., Morales-Molino, C., Revelles, J., Schneider, H., Knaap, W., Leeuwen, J., and Woodbridge, J.: Humans take control of fire-driven diversity changes in Mediterranean Iberia's vegetation during the mid-late Holocene, *The Holocene*, 29, 095968361982665, <https://doi.org/10.1177/0959683619826652>, 2019.
- Cort s S nchez, M., Jim nez Espejo, F. J., Sim n Vallejo, M. D., Gibaja Bao, J. F., Carvalho, A. F., Martinez-Ruiz, F., Gamiz, M. R., Flores, J.-A., Paytan, A., L pez S ez, J. A., Pe a-Chocarro, L., Carri n, J. S., Morales Mu niz, A., Rosell  Izquierdo, E., Riquelme Cantal, J. A., Dean, R. M., Salgueiro, E., Mart nez S nchez, R. M., De la Rubia de Gracia, J. J., Lozano Francisco, M. C., Vera Pel ez, J. L., Rodr guez, L. L., and Bicho, N. F.: The Mesolithic–Neolithic transition in southern Iberia, *Quaternary Res.*, 77, 221–234, <https://doi.org/10.1016/j.yqres.2011.12.003>, 2012.
- Dallmeyer, A., Claussen, M., Lorenz, S. J., and Shanahan, T.: The end of the African humid period as seen by a transient comprehensive Earth system model simulation of the last 8000 years, *Clim. Past*, 16, 117–140, <https://doi.org/10.5194/cp-16-117-2020>, 2020.
- Davis, B. A. S.: Pollen profile N-PEQ, Salada Peque a, Spain. Eur. Pollen Database (EPD), PANGAEA [data set], <https://doi.org/10.1594/PANGAEA.738850>, 2010.
- Davis, B. A. S. and Stevenson, A. C.: The 8.2 ka event and Early–Mid Holocene forests, fires and flooding in the Central Ebro Desert, NE Spain, *Quaternary Sci. Rev.*, 26, 1695–1712, 2007.
- Davis, B. A. S., Brewer, S., Stevenson, A. C., and Guiot, J.: The temperature of Europe during the Holocene reconstructed from pollen data, *Quaternary Sci. Rev.*, 22, 1701–1716, [https://doi.org/10.1016/S0277-3791\(03\)00173-2](https://doi.org/10.1016/S0277-3791(03)00173-2), 2003.
- Davis, T. W., Prentice, I. C., Stocker, B. D., Thomas, R. T., Whitley, R. J., Wang, H., Evans, B. J., Gallego-Sala, A. V., Sykes, M. T., and Cramer, W.: Simple process-led algorithms for simulating habitats (SPLASH v.1.0): robust indices of radiation, evapotranspiration and plant-available moisture, *Geosci. Model Dev.*, 10, 689–708, <https://doi.org/10.5194/gmd-10-689-2017>, 2017.
- de Beaulieu, J.-L., Miras, Y., Andrieu-Ponel, V., and Guiter, F.: Vegetation dynamics in north-western Mediterranean regions: instability of the Mediterranean bioclimate, *Plant Biosyst.*, 139, 114–126, <https://doi.org/10.1080/11263500500197858>, 2005.
- Dorado-Vali o, M., L pez-S ez, J. A., and Garc a-G mez, E.: 21. Patateros, Toledo Mountains (central Spain), *Grana*, 53, 171–173, <https://doi.org/10.1080/00173134.2014.903293>, 2014a.
- Dorado-Vali o, M., L pez-S ez, J. A., and Garc a-G mez, E.: 26. Valdeyernos, Toledo Mountains (central Spain), *Grana*, 53(4), 315–317, <https://doi.org/10.1080/00173134.2014.936490>, 2014b.
- Drake, B. L., Blanco-Gonz lez, A., and Lillios, K. T.: Regional demographic dynamics in the Neolithic Transition in Iberia: Results from summed calibrated date analysis, *J. Archaeol. Method Th.*, 24, 796–812, <https://doi.org/10.1007/s10816-016-9286-y>, 2017.
- Eilers, P. H. and Marx, B. D.: Practical smoothing: The Joys of P-splines, Cambridge University Press, ISBN 9781108482950, 2021.
- Ejarque, A., Juli , R., Reed, J. M., Mesquita-Joanes, F., Marco-Barba, J., and Riera, S.: Coastal evolution in a Mediterranean microtidal zone: Mid to Late Holocene natural dynamics and human management of the Castell  lagoon, NE Spain, *PLoS One*, 11, e0155446, <https://doi.org/10.1371/journal.pone.0155446>, 2016.
- Farquhar, G. D.: Carbon dioxide and vegetation, *Science*, 278, 1411, <https://doi.org/10.1126/science.278.5342.1411>, 1997.
- Franco-M gica, F., Garc a-Ant n, M., Maldonado-Ruiz, J., Morla-Juaristi, C., and Sainz-Ollero, H.: Ancient pine forest on inland dunes in the Spanish northern meseta, *Quaternary Res.*, 63, 1–14, 2005.
- Fyfe, R. M., Woodbridge, J., Palmisano, A., Bevan, A., Shenan, S., Burjachs, F., Legarra Herrero, B., Garc a Puchol, O., Carri n, J. S., Revelles, J., and Roberts, C. N.: Prehistoric palaeodemographics and regional land cover change in eastern Iberia, *The Holocene*, 29, 799–815, <https://doi.org/10.1177/0959683619826643>, 2019.
- Garces-Pastor, S., Canellas-Bolta, N., Clavaguera, A., Calero, M. A., and Vegas-Vilarrubia, T.: Vegetation shifts, human impact and peat bog development in Bassa Nera pond (Central Pyrenees) during the last millennium, *The Holocene*, 27, 553–565, <https://doi.org/10.1177/0959683616670221>, 2017.
- Garc a-Alix, A., Camuera, J., Ramos-Rom n, M. J., Toney, J. L., Sachse, D., Schefu , E., Jim nez-Moreno, G., Jim nez-Espejo, F. J., L pez-Avil s, A., Anderson, R. S., and Yanes, Y.: Paleohydrological dynamics in the Western Mediterranean during the last glacial cycle, *Global Planet. Change*, 202, 103527, <https://doi.org/10.1016/j.gloplacha.2021.103527>, 2021.
- Gerhart, L. M. and Ward, J. K.: Plant responses to low [CO<sub>2</sub>] of the past, *New Phytol.*, 188, 674–695, <https://doi.org/10.1111/j.1469-8137.2010.03441.x>, 2010.
- Gil-Romera, G., Garc a Ant n, M., and Calleja, J. A.: The late Holocene palaeoecological sequence of Serran a de las Villueras (southern Meseta, western Spain), *Veg. Hist. Archaeobot.*, 17, 653–666, 2008.
- Githumbi, E., Fyfe, R., Gaillard, M.-J., Trondman, A.-K., Mazier, F., Nielsen, A.-B., Poska, A., Sugita, S., Woodbridge, J., Azuara, J., Feurdean, A., Grindean, R., Lebreton, V., Marquer, L., Nebout-Combourieu, N., Stan ikait , M., Tan u, I., Tonkov, S., Shumilovskikh, L., and LandClimII data contributors: European pollen-based REVEALS land-cover reconstructions for the Holocene: methodology, mapping and potentials, *Earth Syst. Sci. Data*, 14, 1581–1619, <https://doi.org/10.5194/essd-14-1581-2022>, 2022.
- Gomes, S. D.: 13. Lake Saloio (Nazar , western Portugal), *Grana*, 50, 228–231, 2011.
- Gonz lez, A. V. and Saa, M. P.: Pollen analyse of Holocene peat-bog in the Montes do Buio: Cuadramon (Galice), N. W. of Spain, *Quaternaire*, 11, 257–267, 2000.
- Gonz lez-Samp riz, P., Valero-Garc s, B. L., Moreno, A., Jalut, G., Garc a-Ruiz, J. M., Mart -Bono, C., Delgado-Huertas, A., Navas, A., Otto, T., and Dedoubat, J. J.: Climate vari-

- ability in the Spanish Pyrenees during the last 30,000 yr revealed by the El Portalet sequence, *Quaternary Res.*, 66, 38–52, <https://doi.org/10.1016/j.yqres.2006.02.004>, 2006.
- González-Sampériz, P., Aranbarri, J., Pérez-Sanz, A., Gil-Romera, G., Moreno, A., Leunda, M., Sevilla-Callejo, M., Corella, J. P., Morellón, M., Oliva, B., and Valero-Garcés, B.: Environmental and climate change in the southern Central Pyrenees since the Last Glacial Maximum: A view from the lake records, *Catena*, 149, 668–688, <https://doi.org/10.1016/j.catena.2016.07.041>, 2017.
- Hammer, O., Harper, D., and Ryan, P.: PAST: Paleontological statistics software package for education and data analysis, *Palaeontol. Electron.*, 4, 1–9, 2001.
- Hannon, G.: Late Quaternary vegetation of Sanabria Marsh, North West Spain, Trinity College, Dublin, Ireland, 1985.
- Harrison, S. P.: Modern pollen data for climate reconstructions, version 1 (SMPDS), University of Reading [data set], <https://doi.org/10.17864/1947.194>, 2019.
- Harrison, S. P., Prentice, I. C., Barboni, D., Kohfeld, K. E., Ni, J., and Sutra, J.-P.: Ecophysiological and bioclimatic foundations for a global plant functional classification, *J. Veg. Sci.*, 21, 300–317, <https://doi.org/10.1111/j.1654-1103.2009.01144.x>, 2010.
- Harrison, S. P., Shen, Y., and Sweeney, L.: Pollen data and charcoal data of the Iberian Peninsula (version 3), University of Reading [data set], <https://doi.org/10.17864/1947.000369>, 2022.
- Holden, P. B., Birks, H. J. B., Brooks, S. J., Bush, M. B., Hwang, G. M., Matthews-Bird, F., Valencia, B. G., and van Woesik, R.: BUMPER v1.0: a Bayesian user-friendly model for palaeo-environmental reconstruction, *Geosci. Model Dev.*, 10, 483–498, <https://doi.org/10.5194/gmd-10-483-2017>, 2017.
- Iivonen, L., López-Sáez, J. A., Holmström, L., Alba-Sánchez, F., Pérez-Díaz, S., Carrión, J. S., Ramos-Román, M. J., Camuera, J., Jiménez-Moreno, G., Ruha, L., and Seppä, H.: Spatial and temporal patterns of Holocene precipitation change in the Iberian Peninsula, *Boreas*, 51, 776–792, <https://doi.org/10.1111/bor.12586>, 2022.
- Janssen, C. R. and Woldringh, R. E.: A preliminary radiocarbon dated pollen sequence from the Serra da Estrela, Portugal, *Finisterra*, 16, 299–309, 1981.
- Jiang, W., Guiot, J., Chu, G., Wu, H., Yuan, B., Hatté, C., and Guo, Z.: An improved methodology of the modern analogues technique for palaeoclimate reconstruction in arid and semi-arid regions, *Boreas*, 39, 145–153, <https://doi.org/10.1111/j.1502-3885.2009.00115.x>, 2010.
- Jiménez-Moreno, G., García-Alix, A., Hernández-Corbalán, M. D., Anderson, R. S., and Delgado-Huertas, A.: Vegetation, fire, climate and human disturbance history in the southwestern Mediterranean area during the late Holocene, *Quaternary Res.*, 79, 110–122, <https://doi.org/10.1016/j.yqres.2012.11.008>, 2013.
- Kaufman, D., McKay, N., Routson, C., Erb, M., Davis, B., Heiri, O., Jaccard, S., Tierney, J., Dätwyler, C., Axford, Y., Brussel, T., Cartapanis, O., Chase, B., Dawson, A., de Vernal, A., Engels, S., Jonkers, L., Marsicek, J., Moffa-Sánchez, P., Morrill, C., Orsi, A., Rehfeld, K., Saunders, K., Sommer, P. S., Thomas, E., Tonello, M., Tóth, M., Vachula, R., Andreev, A., Bertrand, S., Biskaborn, B., Bringué, M., Brooks, S., Caniupán, M., Chevalier, M., Cwynar, L., Emile-Geay, J., Fegyveresi, J., Feurdean, A., Finsinger, W., Fortin, M.-C., Foster, L., Fox, M., Gajewski, K., Grosjean, M., Hausmann, S., Heinrichs, M., Holmes, N., Ilyashuk, B., Ilyashuk, E., Juggins, S., Khider, D., Koinig, K., Langdon, P., Larocque-Tobler, I., Li, J., Lotter, A., Luoto, T., Mackay, A., Magyari, E., Malevich, S., Mark, B., Massafiero, J., Montade, V., Nazarova, L., Novenko, E., Pañil, P., Pearson, E., Peros, M., Pienitz, R., Plóciennik, M., Porinchu, D., Potito, A., Rees, A., Reinemann, S., Roberts, S., Rolland, N., Salonen, S., Self, A., Seppä, H., Shala, S., St-Jacques, J.-M., Stenni, B., Strykh, L., Tarrats, P., Taylor, K., van den Bos, V., Velle, G., Wahl, E., Walker, I., Wilmshurst, J., Zhang, E., and Zhilich, S.: A global database of Holocene paleotemperature records, *Sci. Data*, 7, 115, <https://doi.org/10.1038/s41597-020-0445-3>, 2020.
- Leunda, M., González-Sampériz, P., Gil-Romera, G., Aranbarri, J., Moreno, A., Oliva-Urcia, B., Sevilla-Callejo, M., and Valero-Garcés, B.: The Late-Glacial and Holocene Marboré Lake sequence (2612 m a.s.l., Central Pyrenees, Spain): Testing high altitude sites sensitivity to millennial scale vegetation and climate variability, *Global Planet. Change*, 157, 214–231, <https://doi.org/10.1016/j.gloplacha.2017.08.008>, 2017.
- Leunda, M., González-Sampériz, P., Gil-Romera, G., Bartolomé, M., Belmonte-Ribas, Á., Gómez-García, D., Kaltenrieder, P., Juan Manuel Rubiales, C. S., Tinner, W., Morales-Molino, C., and Sancho, C.: Ice cave reveals environmental forcing of long-term Pyrenean tree line dynamics, *J. Ecol.*, 107, 814–828, <https://doi.org/10.1111/1365-2745.13077>, 2019.
- Liu, M.: v0.0.0 ml4418/Iberia-paper: Iberia climate reconstructions, Zenodo [code], <https://doi.org/10.5281/zenodo.7714294>, 2023.
- Liu, M., Prentice, I. C., ter Braak, C. J. F., and Harrison, S. P.: An improved statistical approach for reconstructing past climates from biotic assemblages, *P. R. Soc. A*, 476, <https://doi.org/10.1098/rspa.2020.0346>, 2020.
- López-Merino, L., López-Sáez, J. A., Alba-Sánchez, F., Pérez-Díaz, S., and Carrión, J. S.: 2000 years of pastoralism and fire shaping high-altitude vegetation of Sierra de Gredos in central Spain, *Rev. Palaeobot. Palynol.*, 158, 42–51, <https://doi.org/10.1016/j.revpalbo.2009.07.003>, 2009a.
- López-Merino, L., López-Sáez, J. A., Alba-Sánchez, F., Pérez-Díaz, S., Abel-Schaad, D., and Guerra-Doce, E.: Estudio polínico de una laguna endorreica en Almenara de Adaja (Valladolid, Meseta Norte): Cambios ambientales y actividad humana durante los últimos 2.800 años, *Rev. Española Micropaleontol.*, 41, 333–347, 2009b.
- López-Merino, L., Cortizas, A. M., and López-Sáez, J. A.: Early agriculture and palaeoenvironmental history in the North of the Iberian Peninsula: a multi-proxy analysis of the Monte Areo mire (Asturias, Spain), *J. Archaeol. Sci.*, 37, 1978–1988, <https://doi.org/10.1016/j.jas.2010.03.003>, 2010.
- López-Merino, L., Cortizas, A. M., and López-Sáez, J. A.: Human-induced changes on wetlands: A study case from NW Iberia, *Quaternary Sci. Rev.*, 30, 2745–2754, 2011.
- López-Merino, L., Silva-Sánchez, N., Kaal, J., López-Sáez, J. A., and Martínez-Cortizas, A.: Post-disturbance vegetation dynamics during the Late Pleistocene and the Holocene: An example from NW Iberia, *Glob. Planet. Change*, 92–93, 58–70, <https://doi.org/10.1016/j.gloplacha.2012.04.003>, 2012.
- López-Sáez, J. A. and López-Merino, L.: Coprophilous fungi as a source of information of anthropic activities during the Prehistory in the Amblés Valley (Ávila, Spain): The archaeopalynological record, *Rev. Esp. Micropaleontol.*, 38, 49–75, 2007.

- López-Sáez, J. A., Sánchez, M., and López, P.: Evolución del Lanzahíta (Valle del Tiétar, vila) durante el Holoceno reciente: Una interpretación palinológica, *Trasierra*, 1999, 81–86, 1999.
- López-Sáez, J. A., López-Merino, L., Mateo, M. Á., Serrano, Ó., Pérez-Díaz, S., and Serrano, L.: Palaeoecological potential of the marine organic deposits of Posidonia oceanica: A case study in the NE Iberian Peninsula, *Palaeogeogr. Palaeoclimatol. Palaeoecol.*, 271, 215–224, <https://doi.org/10.1016/j.palaeo.2008.10.020>, 2009.
- López-Sáez, J. A., López-Merino, L., Alba-Sánchez, F., Pérez-Díaz, S., Abel-Schaad, D., and Carrión, J. S.: Late Holocene ecological history of *Pinus pinaster* forests in the Sierra de Gredos of central Spain, *Plant Ecol.*, 206, 195–209, <https://doi.org/10.1007/s11258-009-9634-z>, 2010.
- López-Sáez, J. A., Abel-Schaad, D., Alba-Sánchez, F., González-Pellejero, R., Frochoso, M., and Allende, F.: 20. Culazón, Cantabrian Mountains (northern Spain), *Grana*, 52, 316–318, 2013.
- López-Sáez, J. A., Abel-Schaad, D., Robles-López, S., Pérez-Díaz, S., Alba-Sánchez, F., and Nieto-Lugilde, D.: Landscape dynamics and human impact on high-mountain woodlands in the western Spanish Central System during the last three millennia, *J. Archaeol. Sci. Reports*, 9, 203–218, <https://doi.org/10.1016/j.jasrep.2016.07.027>, 2016.
- López-Sáez, J. A., Figueiral, I., and Cruz, D.: Palaeoenvironment and vegetation dynamics in serra da Nave (Alto Paiva, Beira Alta, Portugal), during the Late Pleistocene and the Holocene, in: *Actas da Mesa-Redonda “A Pré-história e a Proto-história no Centro de Portugal: avaliação e perspectivas de futuro”* (Mangualde, Novembro de 2011), edited by: Cruz, D. J., Centro de Estudos Pré-históricos da Beira Alta, [https://www.researchgate.net/publication/322860918\\_Palaeoenvironment\\_and\\_vegetation\\_dynamics\\_in\\_serra\\_da\\_Nave\\_Alto\\_Paiva\\_Beira\\_Alta\\_Portugal\\_during\\_the\\_Late\\_Pleistocene\\_and\\_the\\_Holocene](https://www.researchgate.net/publication/322860918_Palaeoenvironment_and_vegetation_dynamics_in_serra_da_Nave_Alto_Paiva_Beira_Alta_Portugal_during_the_Late_Pleistocene_and_the_Holocene) (last access: 10 March 2023), 2017.
- López-Sáez, J. A., Pérez-Díaz, S., Rodríguez-Ramírez, A., Blanco-González, A., Villarías-Robles, J. J. R., Luelmo-Lautenschlaeger, R., Jiménez-Moreno, G., Celestino-Pérez, S., Cerrillo-Cuenca, E., Pérez-Asensio, J. N., and León, Á.: Mid-late Holocene environmental and cultural dynamics at the south-west tip of Europe (Doñana National Park, SW Iberia, Spain), *J. Archaeol. Sci. Reports*, 22, 58–78, <https://doi.org/10.1016/j.jasrep.2018.09.014>, 2018a.
- López-Sáez, J. A., Vargas, G., Ruiz-Fernández, J., Blarquez, O., Alba-Sánchez, F., Oliva, M., Pérez-Díaz, S., Robles-López, S., and Abel-Schaad, D.: Paleofire dynamics in Central Spain during the Late Holocene: The role of climatic and anthropogenic forcing, *Land Degrad. Dev.*, 29, 2045–2059, <https://doi.org/10.1002/ldr.2751>, 2018b.
- López-Sáez, J. A., Carrasco, R. M., Turu, V., Ruiz-Zapata, B., Gil-García, M. J., Luelmo-Lautenschlaeger, R., Pérez-Díaz, S., Alba-Sánchez, F., Abel-Schaad, D., Ros, X., and Pedraza, J.: Late Glacial-early holocene vegetation and environmental changes in the western Iberian Central System inferred from a key site: The Navamuño record, Béjar range (Spain), *Quaternary Sci. Rev.*, 230, 106167, <https://doi.org/10.1016/j.quascirev.2020.106167>, 2020.
- Luelmo-Lautenschlaeger, R., López-Sáez, J. A., and Pérez-Díaz, S.: 39. Las Lanchas, Toledo Mountains (central Spain), *Grana*, 57, 246–248, <https://doi.org/10.1080/00173134.2017.1366547>, 2018a.
- Luelmo-Lautenschlaeger, R., López-Sáez, J. A., and Pérez-Díaz, S.: Contributions to the European Pollen Database. Botija, Toledo Mountains (central Spain), *Grana*, 57, 322–324, <https://doi.org/10.1080/00173134.2017.1400587>, 2018b.
- Luelmo-Lautenschlaeger, R., Pérez-Díaz, S., Alba-Sánchez, F., Abel-Schaad, D., and López-Sáez, J. A.: Vegetation history in the Toledo Mountains (central Iberia): human impact during the last 1300 years, *Sustainability*, 10, 2575, <https://doi.org/10.3390/su10072575>, 2018c.
- Luelmo-Lautenschlaeger, R., Blarquez, O., Pérez-Díaz, S., Morales-Molino, C., and López-Sáez, J. A.: The Iberian Peninsula’s Burning Heart: Long-term fire history in the Toledo Mountains (Central Spain), *Fire*, 2, 54, <https://doi.org/10.3390/fire2040054>, 2019a.
- Luelmo-Lautenschlaeger, R., Pérez-Díaz, S., Blarquez, O., Morales-Molino, C., and López-Sáez, J. A.: The Toledo Mountains: A resilient landscape and a landscape for resilience? Hazards and strategies in a mid-elevation mountain region in Central Spain, *Quaternary*, 2, 35, <https://doi.org/10.3390/quat2040035>, 2019b.
- Manzano, S., Carrión, J. S., López-Merino, L., Jiménez-Moreno, G., Toney, J. L., Armstrong, H., Anderson, R. S., García-Alix, A., Pérez, J. L. G., and Sánchez-Mata, D.: A palaeoecological approach to understanding the past and present of Sierra Nevada, a Southwestern European biodiversity hotspot, *Global Planet. Change*, 175, 238–250, <https://doi.org/10.1016/j.gloplacha.2019.02.006>, 2019.
- Mariscal, B.: Comparación palinológica entre una turbera de la cordillera central y unas turberas de la cordillera cantábrica, in: *II. European Paleobot*, Universidad Complutense Madrid, Madrid, p. 28, 1989.
- Mariscal, B.: Variación de la vegetación holocena (4300–280 B. P.) de Cantabria a través del análisis polínico de la turbera del Alsa, *Estud. Geol.-Madrid*, 49, 63–69, 1993.
- Mariscal-Álvarez, B.: Estudio polínico de la turbera del Cueto de la Avellanosa, Polaciones (Cantabria), *VI Reunión do grupo español de traballo de Cuaternario*, *Cuad. do Lab. xeolóxico laxe*, 5, 205–226, 1983.
- Mariscal-Álvarez, B.: Análisis polínico de la turbera del Pico del Sertal, de la Sierra de Paña Sagra. Reconstrucción de la paleoflora y de la paleoclimatología durante el Holoceno en la zona central de la Cordillera Cantábrica, in: *Quaternary Climate in Western Mediterranean*, edited by: Lopez-Vera, F., Universidad Autónoma, Madrid, <https://library.metoffice.gov.uk/portal/Default/en-GB/RecordView/Index/254554> (last access: 10 March 2023), 1986.
- Martín-Puertas, C., Valero-Garcés, B. L., Pilar Mata, M., González-Sampériz, P., Bao, R., Moreno, A., and Stefanova, V.: Arid and humid phases in southern Spain during the last 4000 years: the Zoñar Lake record, Córdoba, *The Holocene*, 18, 907–921, <https://doi.org/10.1177/0959683608093533>, 2008.
- Martínez-Cortizas, A., Costa-Casais, M., and López-Sáez, J. A.: Environmental change in NW Iberia between 7000 and 500 cal BC, *Quatern. Int.*, 200, 77–89, <https://doi.org/10.1016/j.quaint.2008.07.012>, 2009.

- Mateus, J. E.: The coastal lagoon region near Carvalhal during the Holocene; some geomorphological aspects derived from palaeoecological study at Lagoa Travessa, in: *Actas da I Reunião do Quaternário Ibérica*, Organizadora da I Reunião do Quaternário Ibérico, 237–250, 1985.
- Mateus, J. E.: Lagoa Travessa: A Holocene pollen diagram from the south-west coast of Portugal, *Rev. Biol.*, 14, 17–94, 1989.
- Mauri, A., Davis, B. A. S., Collins, P. M., and Kaplan, J. O.: The influence of atmospheric circulation on the mid-Holocene climate of Europe: a data–model comparison, *Clim. Past*, 10, 1925–1938, <https://doi.org/10.5194/cp-10-1925-2014>, 2014.
- Mauri, A., Davis, B. A. S., Collins, P. M., and Kaplan, J. O.: The climate of Europe during the Holocene: A gridded pollen-based reconstruction and its multiproxy evaluation, *Quaternary Sci. Rev.*, 112, 109–127, <https://doi.org/10.1016/j.quascirev.2015.01.013>, 2015.
- McKeever, M.: Comparative palynological studies of two lake sites in western Ireland and northwestern Spain, Trinity College, Dublin, Ireland, 1984.
- Mighall, T. M., Martínez Cortizas, A., Biester, H., and Turner, S. E.: Proxy climate and vegetation changes during the last five millennia in NW Iberia: Pollen and non-pollen palynomorph data from two ombrotrophic peat bogs in the North Western Iberian Peninsula, *Rev. Palaeobot. Palyno.*, 141, 203–223, <https://doi.org/10.1016/j.revpalbo.2006.03.013>, 2006.
- Miras, Y., Ejarque, A., Riera, S., Martínez, J. M., Orengo, H., and Euba, I.: Dynamique holocène de la végétation et occupation des Pyrénées andorranes depuis le Néolithique ancien, d’après l’analyse pollinique de la tourbière de Bosc dels Estanyons (2180 m, Vall del Madriu, Andorre), *C. R. Palevol.*, 6, 291–300, <https://doi.org/10.1016/j.crpv.2007.02.005>, 2007.
- Miras, Y., Ejarque, A., Orengo, H., Mora, S. R., Palet, J. M., and Poiraud, A.: Prehistoric impact on landscape and vegetation at high altitudes: An integrated palaeoecological and archaeological approach in the eastern Pyrenees (Perafita valley, Andorra), *Plant Biosyst.*, 144, 924–939, <https://doi.org/10.1080/11263504.2010.491980>, 2010.
- Miras, Y., Ejarque, A., Riera, S., Orengo, H. A., and Palet Martínez, J. M.: 28. Andorran high Pyrenees (Perafita Valley, Andorra): SerraMijtana fen, *Grana*, 54, 313–316, <https://doi.org/10.1080/00173134.2015.1087590>, 2015.
- Moe, D. and van der Knaap, W. O.: Transhumance in mountain areas: Additional interpretation of three pollen diagrams from Norway, Portugal and Switzerland, in: *Pact*, vol. 31, edited by: Moe, D. and Hicks, S., European Study Group on Physical, Chemical and Mathematical Techniques Applied to Archaeology, Strasbourg, France, 91–103, ISSN 0257-8727 1990.
- Morales-Molino, C. and García-Antón, M.: Vegetation and fire history since the last glacial maximum in an inland area of the western Mediterranean Basin (Northern Iberian Plateau, NW Spain), *Quaternary Res.*, 81, 63–77, 2014.
- Morales-Molino, C., García Antón, M., and Morla, C.: Late Holocene vegetation dynamics on an Atlantic-Mediterranean mountain in NW Iberia, *Palaeogeogr. Palaeoclimatol. Palaeoecol.*, 302, 323–337, <https://doi.org/10.1016/j.palaeo.2011.01.020>, 2011.
- Morales-Molino, C., García-Antón, M., Postigo-Mijarra, J. M., and Morla, C.: Holocene vegetation, fire and climate interactions on the westernmost fringe of the Mediterranean Basin, *Quaternary Sci. Rev.*, 59, 5–17, 2013.
- Morales-Molino, C., Colombaroli, D., Valbuena-Carabaña, M., Tinner, W., Salomón, R. L., Carrión, J. S., and Gil, L.: Land-use history as a major driver for long-term forest dynamics in the Sierra de Guadarrama National Park (central Spain) during the last millennia: implications for forest conservation and management, *Global Planet. Change*, 152, 64–75, <https://doi.org/10.1016/j.gloplacha.2017.02.012>, 2017a.
- Morales-Molino, C., Tinner, W., García-Antón, M., and Colombaroli, D.: The historical demise of *Pinus nigra* forests in the Northern Iberian Plateau (south-western Europe), *J. Ecol.*, 105, 634–646, 2017b.
- Morales-Molino, C., Colombaroli, D., Tinner, W., Perea, R., Valbuena-Carabaña, M., Carrión, J. S., and Gil, L.: Vegetation and fire dynamics during the last 4000 years in the Cabañeros National Park (central Spain), *Rev. Palaeobot. Palyno.*, 253, 110–122, <https://doi.org/10.1016/j.revpalbo.2018.04.001>, 2018.
- Morales-Molino, C., Tinner, W., Perea, R., Carrión, J. S., Colombaroli, D., Valbuena-Carabaña, M., Zafra, E., and Gil, L.: Unprecedented herbivory threatens rear-edge populations of *Betula* in southwestern Eurasia, *Ecology*, 100, e02833, <https://doi.org/10.1002/ecy.2833>, 2019.
- Morellón, M., Valero-Garcés, B., González-Sampérez, P., Vegas-Vilarrúbia, T., Rubio, E., Rieradevall, M., Delgado-Huertas, A., Mata, P., Romero, Ó., Engstrom, D. R., López-Vicente, M., Navas, A., and Soto, J.: Climate changes and human activities recorded in the sediments of Lake Estanya (NE Spain) during the Medieval Warm Period and Little Ice Age, *J. Paleolimnol.*, 46, 423–452, <https://doi.org/10.1007/s10933-009-9346-3>, 2011.
- Morellón, M., Aranbarri, J., Moreno, A., González-Sampérez, P., and Valero-Garcés, B. L.: Early Holocene humidity patterns in the Iberian Peninsula reconstructed from lake, pollen and speleothem records, *Quaternary Sci. Rev.*, 181, 1–18, <https://doi.org/10.1016/j.quascirev.2017.11.016>, 2018.
- Moreno, A., López-Merino, L., Leira, M., Marco-Barba, J., González-Sampérez, P., Valero-Garcés, B. L., López-Sáez, J. A., Santos, L., Mata, P., and Ito, E.: Revealing the last 13,500 years of environmental history from the multiproxy record of a mountain lake (Lago Enol, northern Iberian Peninsula), *J. Paleolimnol.*, 46, 327–349, <https://doi.org/10.1007/s10933-009-9387-7>, 2011.
- Múgica, F. F., Antón, M. G., Ruiz, J. M., Juaristi, C. M., and Ollerol, H. S.: The Holocene history of *Pinus* forests in the Spanish Northern Meseta, *The Holocene*, 11, 343–358, <https://doi.org/10.1191/095968301669474913>, 2001.
- Muñoz Sobrino, C., Heiri, O., Hazekamp, M., van der Velden, D., Kirilova, E. P., García-Moreiras, I., and Lotter, A. F.: New data on the Lateglacial period of SW Europe: a high resolution multiproxy record from Laguna de la Roya (NW Iberia), *Quaternary Sci. Rev.*, 80, 58–77, <https://doi.org/10.1016/j.quascirev.2013.08.016>, 2013.
- New, M., Lister, D., and Hulme, M.: A high-resolution data set of surface climate over global land areas, *Clim. Res.*, 21, 1–25, 2002.
- Overpeck, J. T., Webb, T., and Prentice, I. C.: Quantitative interpretation of fossil pollen spectra: Dissimilarity coefficients and the method of modern analogs, *Quaternary Res.*, 23, 87–108, [https://doi.org/10.1016/0033-5894\(85\)90074-2](https://doi.org/10.1016/0033-5894(85)90074-2), 1985.

- Pantaléon-Cano, J., Yll, E.-I., Pérez-Obiol, R., and Roure, J. M.: Palynological evidence for vegetational history in semi-arid areas of the western Mediterranean (Almería, Spain), *The Holocene*, 13, 109–119, <https://doi.org/10.1191/0959683603hl598rp>, 2003.
- Parker, S. E., Harrison, S. P., and Braconnot, P.: Speleothem records of monsoon interannual–interdecadal variability through the Holocene, *Environ. Res. Commun.*, 3, 121002, <https://doi.org/10.1088/2515-7620/ac3eaa>, 2021.
- Peñalba Garmendia, M. C.: Dynamique de végétation tardiglaciaire et holocène du Centre-Nord de l'Espagne d'après l'analyse pollinique, Aix-Marseille 3, <https://www.theses.fr/1989AIX30033> (last access: 10 March 2023), 1989.
- Penalba, M. C.: The history of the Holocene vegetation in northern Spain from pollen analysis, *J. Ecol.*, 82, 815, <https://doi.org/10.2307/2261446>, 1994.
- Peña-Chocarro, L., Peña, L. Z., Gazólaz, J. G., Morales, M. G., Sesma, J. S., and Straus, L. G.: The spread of agriculture in northern Iberia: new archaeobotanical data from El Mirón cave (Cantabria) and the open-air site of Los Cascajos (Navarra), *Veg. Hist. Archaeobot.*, 14, 268–278, <https://doi.org/10.1007/s00334-005-0078-7>, 2005.
- Pérez-Díaz, S. and López-Sáez, J. A.: 33. Verdeospesoa mire (Basque Country, Northern Iberian Peninsula, Spain), *Grana*, 56, 315–317, 2017.
- Pérez-Díaz, S., López-Sáez, J. A., Núñez de la Fuente, S., and Ruiz-Alonso, M.: Early farmers, megalithic builders and the shaping of the cultural landscapes during the Holocene in Northern Iberian mountains. A palaeoenvironmental perspective, *J. Archaeol. Sci. Reports*, 18, 463–474, 2018.
- Pérez-Obiol, R. and Julià, R.: Climatic change on the Iberian peninsula recorded in a 30,000-yr pollen record from lake Banyoles, *Quaternary Res.*, 41, 91–98, <https://doi.org/10.1006/qres.1994.1010>, 1994.
- Pérez-Obiol, R., Bal, M. C., Pèlachs, A., Cunill, R., and Soriano, J. M.: Vegetation dynamics and anthropogenically forced changes in the Estanilles peat bog (southern Pyrenees) during the last seven millennia, *Veg. Hist. Archaeobot.*, 21, 385–396, 2012.
- Pérez-Obiol, R., Roure, J. M., Pantaléon-Cano, J., and Yll, E. I.: Análisis polínico de una secuencia holocénica en Roquetas de Mar (Almería), in: *Trabajos de Palinología básica y aplicada, X Simposio de Palinología, APLE, Valencia, septiembre 1994*, 189–198, Universitat de València, <https://dialnet.unirioja.es/servlet/articulo?codigo=1387752> (last access: 10 March 2023), 1994.
- Pérez-Obiol, R., Bal, M. C., Pèlachs, A., Cunill, R., and Soriano, J. M.: Vegetation dynamics and anthropogenically forced changes in the Estanilles peat bog (southern Pyrenees) during the last seven millennia, *Veg. Hist. Archaeobot.*, 21, 385–396, <https://doi.org/10.1007/s00334-012-0351-5>, 2012.
- Pérez-Sanz, A., González-Sampériz, P., Moreno, A., Valero-Garcés, B., Gil-Romera, G., Rieradevall, M., Tarrats, P., Lasheras-Álvarez, L., Morellón, M., Belmonte, A., Sancho, C., Sevilla-Callejo, M., and Navas, A.: Holocene climate variability, vegetation dynamics and fire regime in the central Pyrenees: the Basa de la Mora sequence (NE Spain), *Quaternary Sci. Rev.*, 73, 149–169, <https://doi.org/10.1016/j.quascirev.2013.05.010>, 2013.
- Peyron, O., Guiot, J., Cheddadi, R., Tarasov, P., Reille, M., De Beaulieu, J.-L., Bottema, S., and Andrieu, V.: Climatic reconstruction in Europe for 18,000 yr B.P. from pollen data, *Quaternary Res.*, 49, 183–196, <https://doi.org/10.1006/qres.1997.1961>, 1998.
- Prentice, I. C. and Harrison, S. P.: Ecosystem effects of CO<sub>2</sub> concentration: evidence from past climates, *Clim. Past*, 5, 297–307, <https://doi.org/10.5194/cp-5-297-2009>, 2009.
- Prentice, I. C., Meng, T., Wang, H., Harrison, S. P., Ni, J., and Wang, G.: Evidence of a universal scaling relationship for leaf CO<sub>2</sub> drawdown along an aridity gradient, *New Phytol.*, 190, 169–180, <https://doi.org/10.1111/j.1469-8137.2010.03579.x>, 2011.
- Prentice, I. C., Cleator, S. F., Huang, Y. H., Harrison, S. P., and Roulstone, I.: Reconstructing ice-age palaeoclimates: Quantifying low-CO<sub>2</sub> effects on plants, *Global Planet. Change*, 149, 166–176, <https://doi.org/10.1016/j.gloplacha.2016.12.012>, 2017.
- Prentice, I. C., Villegas-Díaz, R., and Harrison, S. P.: Accounting for atmospheric carbon dioxide variations in pollen-based reconstruction of past hydroclimates, *Global Planet. Change*, 211, 103790, <https://doi.org/10.1016/j.gloplacha.2022.103790>, 2022.
- Ramos-Román, M. J., Jiménez-Moreno, G., Anderson, R. S., García-Alix, A., Toney, J. L., Jiménez-Espejo, F. J., and Carrión, J. S.: Centennial-scale vegetation and North Atlantic Oscillation changes during the Late Holocene in the southern Iberia, *Quaternary Sci. Rev.*, 143, 84–95, <https://doi.org/10.1016/j.quascirev.2016.05.007>, 2016.
- Ramos-Román, M. J., Jiménez-Moreno, G., Camuera, J., García-Alix, A., Anderson, R., Jiménez-Espejo, F., Sachse, D., Jaime, T., Carrión, J., Webster, C., and Yanes, Y.: Millennial-scale cyclical environment and climate variability during the Holocene in the western Mediterranean region deduced from a new multi-proxy analysis from the Padul record (Sierra Nevada, Spain), *Global Planet. Change*, 168, 35–53, <https://doi.org/10.1016/j.gloplacha.2018.06.003>, 2018.
- Reimer, P. J., Austin, W. E. N., Bard, E., Bayliss, A., Blackwell, P. G., Bronk Ramsey, C., Butzin, M., Cheng, H., Edwards, R. L., Friedrich, M., Grootes, P. M., Guilderson, T. P., Hajdas, I., Heaton, T. J., Hogg, A. G., Hughen, K. A., Kromer, B., Manning, S. W., Muscheler, R., Palmer, J. G., Pearson, C., Van Der Plicht, J., Reimer, R. W., Richards, D. A., Scott, E. M., Southon, J. R., Turney, C. S. M., Wacker, L., Adolphi, F., Büntgen, U., Capano, M., Fahrni, S. M., Fogtmann-Schulz, A., Friedrich, R., Köhler, P., Kudsk, S., Miyake, F., Olsen, J., Reinig, F., Sakamoto, M., Sookdeo, A., and Talamo, S.: The IntCal20 Northern Hemisphere radiocarbon age calibration curve (0–55 cal k BP), *Radiocarbon*, 62, 725–757, <https://doi.org/10.1017/RDC.2020.41>, 2020.
- Revelles, J., Cho, S., Iriarte, E., Burjachs, F., van Geel, B., Palomo, A., Piqué, R., Peña-Chocarro, L., and Terradas, X.: Mid-Holocene vegetation history and Neolithic land-use in the Lake Banyoles area (Girona, Spain), *Palaeogeogr. Palaeoclimatol. Palaeoecol.*, 435, 70–85, <https://doi.org/10.1016/j.palaeo.2015.06.002>, 2015.
- Revelles, J., Burjachs, F., Palomo, A., Piqué, R., Iriarte, E., Pérez-Obiol, R., and Terradas, X.: Human-environment interaction during the Mesolithic-Neolithic transition in the NE Iberian Peninsula. Vegetation history, climate change and human impact during the Early-Middle Holocene in the Eastern Pre-Pyrenees, *Quaternary Sci. Rev.*, 184, 183–200, <https://doi.org/10.1016/j.quascirev.2017.08.025>, 2018.

- Robles-López, S., Manzano-Rodríguez, S., Pérez-Díaz, S., and López-Sáez, J. A.: 35. Labradillos mire, Gregos Range (central Spain), Grana, 56, 398–400, <https://doi.org/10.1080/00173134.2017.1282976>, 2017a.
- Robles-López, S., Luelmo-Lautenschlaeger, R., Pérez-Díaz, S., Abel-Schaad, D., Alba-Sánchez, F., Ruiz-Alonso, M., and López-Sáez, J. A.: Vulnerabilidad y resiliencia de los pinares de alta montaña de la Sierra de Gredos (Ávila, sistema central): Dos mil años de dinámica socioecológica, Cuaternario y Geomorf., 31, 51–72, <https://doi.org/10.17735/cyg.v31i3-4.55594>, 2017b.
- Robles-López, S., Fernández Martín-Consuegra, A., Pérez-Díaz, S., Alba-Sánchez, F., Broothaerts, N., Abel-Schaad, D., and López-Sáez, J. A.: The dialectic between deciduous and coniferous forests in central Iberia: A palaeoenvironmental perspective during the late Holocene in the Gredos range, Quatern. Int., 470, 148–165, <https://doi.org/10.1016/j.quaint.2017.05.012>, 2018.
- Robles-López, S., Pérez-Díaz, S., Ruiz-Alonso, M., Blarquez, O., Luelmo-Lautenschlaeger, R., and López-Sáez, J. A.: Holocene vegetation and fire dynamics in the supra-Mediterranean belt of the Gredos Range (central Iberian Peninsula), Plant Biosyst., 154, 74–86, <https://doi.org/10.1080/11263504.2019.1578281>, 2020.
- Salonen, J. S., Ilvonen, L., Seppä, H., Holmström, L., Telford, R. J., Gaidamavičius, A., Stančikaitė, M., and Subetto, D.: Comparing different calibration methods (WA/WA-PLS regression and Bayesian modelling) and different-sized calibration sets in pollen-based quantitative climate reconstruction, The Holocene, 22, 413–424, <https://doi.org/10.1177/0959683611425548>, 2011.
- Salonen, J. S., Korpela, M., Williams, J. W., and Luoto, M.: Machine-learning based reconstructions of primary and secondary climate variables from North American and European fossil pollen data, Sci. Rep.-UK, 9, 15805, <https://doi.org/10.1038/s41598-019-52293-4>, 2019.
- Sanchez-Goñi, M. F. and Hannon, G. E.: High-altitude vegetational pattern on the Iberian Mountain Chain (north-central Spain) during the Holocene, The Holocene, 9, 39–57, <https://doi.org/10.1191/095968399671230625>, 1999.
- Schneider, H., Höfer, D., Trog, C., Busch, S., Schneider, M., Baade, J., Daut, G., and Mäusbacher, R.: Holocene estuary development in the Algarve Region (Southern Portugal) – A reconstruction of sedimentological and ecological evolution, Quatern. Int., 221, 141–158, <https://doi.org/10.1016/j.quaint.2009.10.004>, 2010.
- Schneider, H., Höfer, D., Trog, C., and Mäusbacher, R.: Holocene landscape development along the Portuguese Algarve coast – A high resolution palynological approach, Quatern. Int., 407, 47–63, <https://doi.org/10.1016/j.quaint.2016.02.039>, 2016.
- Schröder, T., López-Sáez, J. A., van't Hoff, J., and Reichert, K.: Unravelling the Holocene environmental history of south-western Iberia through a palynological study of Lake Medina sediments, The Holocene, 30, 13–22, <https://doi.org/10.1177/0959683619865590>, 2019.
- Shen, Y., Sweeney, L., Liu, M., Lopez Saez, J. A., Pérez-Díaz, S., Luelmo-Lautenschlaeger, R., Gil-Romera, G., Hofer, D., Jiménez-Moreno, G., Schneider, H., Prentice, I. C., and Harrison, S. P.: Reconstructing burnt area during the Holocene: an Iberian case study, Clim. Past, 18, 1189–1201, <https://doi.org/10.5194/cp-18-1189-2022>, 2022.
- Silva-Sánchez, N., Martínez Cortizas, A., Abel-Schaad, D., López-Sáez, J. A., and Mighall, T. M.: Influence of climate change and human activities on the organic and inorganic composition of peat during the 'Little Ice Age' (El Payo mire, W Spain), The Holocene, 26, 1290–1303, <https://doi.org/10.1177/0959683616638439>, 2016.
- Stefanini, B.: A comparison of climate and vegetation dynamics in central Ireland and NW Spain since the mid-Holocene, University of Dublin, Trinity College, Dublin, Ireland, <http://hdl.handle.net/2262/78629> (last access: 10 March 2023), 2008.
- Stevenson, A. C.: The Holocene forest history of the Montes Universales, Teruel, Spain, The Holocene, 10, 603–610, <https://doi.org/10.1191/095968300670543500>, 2000.
- Stoll, H. M., Moreno, A., Mendez-Vicente, A., Gonzalez-Lemos, S., Jimenez-Sanchez, M., Dominguez-Cuesta, M. J., Edwards, R. L., Cheng, H., and Wang, X.: Paleoclimate and growth rates of speleothems in the northwestern Iberian Peninsula over the last two glacial cycles, Quaternary Res., 80, 284–290, <https://doi.org/10.1016/j.yqres.2013.05.002>, 2013.
- Tarrats, P., Heiri, O., Valero-Garcés, B., Cañedo-Argüelles, M., Prat, N., Rieradevall, M., and González-Sampérez, P.: Chironomid-inferred Holocene temperature reconstruction in Basa de la Mora Lake (Central Pyrenees), The Holocene, 28, 1685–1696, <https://doi.org/10.1177/0959683618788662>, 2018.
- Tarrosó, P., Carrión, J., Dorado-Valiño, M., Queiroz, P., Santos, L., Valdeolmillos-Rodríguez, A., Célio Alves, P., Brito, J. C., and Cheddadi, R.: Spatial climate dynamics in the Iberian Peninsula since 15 000 yrBP, Clim. Past, 12, 1137–1149, <https://doi.org/10.5194/cp-12-1137-2016>, 2016.
- ter Braak, C. J. F. and Juggins, S.: Weighted averaging partial least squares regression (WA-PLS): An improved method for reconstructing environmental variables from species assemblages, Hydrobiologia, 269, 485–502, <https://doi.org/10.1007/BF00028046>, 1993.
- Thatcher, D. L., Wanamaker, A. D., Denniston, R. F., Asmerom, Y., Polyak, V. J., Fullick, D., Ummenhofer, C. C., Gillikin, D. P., and Haws, J. A.: Hydroclimate variability from western Iberia (Portugal) during the Holocene: Insights from a composite stalagmite isotope record, The Holocene, 30, 966–981, <https://doi.org/10.1177/0959683620908648>, 2020.
- Trondman, A.-K., Gaillard, M.-J., Mazier, F., Sugita, S., Fyfe, R., Nielsen, A. B., Twiddle, C., Barratt, P., Birks, H. J. B., Bjune, A. E., Björkman, L., Broström, A., Caseldine, C., David, R., Dodson, J., Dörfler, W., Fischer, E., van Geel, B., Giesecke, T., Hultberg, T., Kalnina, L., Kangur, M., van der Knaap, P., Koff, T., Kuneš, P., Lagerås, P., Latalowa, M., Lechterbeck, J., Leroyer, C., Leydet, M., Lindbladh, M., Marquer, L., Mitchell, F. J. G., Odgaard, B. V., Peglar, S. M., Persson, T., Poska, A., Rösch, M., Seppä, H., Veski, S., and Wick, L.: Pollen-based quantitative reconstructions of Holocene regional vegetation cover (plant-functional types and land-cover types) in Europe suitable for climate modelling, Glob. Change Biol., 21, 676–697, <https://doi.org/10.1111/gcb.12737>, 2015.
- Turner, C. and Hannon, G. E.: Vegetational evidence for late Quaternary climatic changes in southwest Europe in relation to the influence of the North Atlantic Ocean, Philos. T. Roy. Soc. B, 318, 451–485, <https://doi.org/10.1098/rstb.1988.0019>, 1988.
- Valero-Garcés, B. L., Navas, A., Machin, J., Stevenson, T., and Davis, B.: Responses of a saline lake ecosystem in a semiarid region to irrigation and climate variability, Ambio A J. Hum. Env-

- iron., 29, 344–350, <https://doi.org/10.1579/0044-7447-29.6.344>, 2000.
- van den Brink, L. M. and Janssen, C. R.: The effect of human activities during cultural phases on the development of montane vegetation in the Serra de Estrela, Portugal, *Rev. Palaeobot. Palynol.*, 44, 193–215, [https://doi.org/10.1016/0034-6667\(85\)90016-8](https://doi.org/10.1016/0034-6667(85)90016-8), 1985.
- van der Knaap, W. O. and van Leeuwen, J. F. N.: Holocene vegetation, human impact, and climatic change in the Serra da Estrela, Portugal, *Diss. Bot.*, 234, 497–535, <https://doi.org/10.7892/boris.81078>, 1984.
- van der Knaap, W. O. and van Leeuwen, J. F. N.: Holocene vegetation succession and degradation as responses to climatic change and human activity in the Serra de Estrela, Portugal, *Rev. Palaeobot. Palynol.*, 89, 153–211, [https://doi.org/10.1016/0034-6667\(95\)00048-0](https://doi.org/10.1016/0034-6667(95)00048-0), 1995.
- van der Knaap, W. O. and van Leeuwen, J. F. N.: Late Glacial and early Holocene vegetation succession, altitudinal vegetation zonation, and climatic change in the Serra da Estrela, Portugal, *Rev. Palaeobot. Palynol.*, 97, 239–285, [https://doi.org/10.1016/S0034-6667\(97\)00008-0](https://doi.org/10.1016/S0034-6667(97)00008-0), 1997.
- Villegas-Díaz, R., Cruz-Silva, E., and Harrison, S. P.: ageR: Supervised age models, Zenodo, <https://doi.org/10.5281/zenodo.4636715>, 2021.
- von Engelbrechten, S.: Late-glacial and Holocene vegetation and environmental history of the Sierra de Urbiión, PhD thesis, North-West Central Spain, Trinity College, Dublin, Ireland, 1999.
- Walczak, I. W., Baldini, J. U. L., Baldini, L. M., McDermott, F., Marsden, S., Standish, C. D., Richards, D. A., Andreo, B., and Slater, J.: Reconstructing high-resolution climate using CT scanning of unsectioned stalagmites: A case study identifying the mid-Holocene onset of the Mediterranean climate in southern Iberia, *Quaternary Sci. Rev.*, 127, 117–128, <https://doi.org/10.1016/j.quascirev.2015.06.013>, 2015.
- Wei, D., González-Sampériz, P., Gil-Romera, G., Harrison, S. P., and Prentice, I. C.: Seasonal temperature and moisture changes in interior semi-arid Spain from the last interglacial to the Late Holocene, *Quaternary Res.*, 101, 143–155, <https://doi.org/10.1017/qua.2020.108>, 2021.
- Wu, H., Guiot, J., Brewer, S., and Guo, Z.: Climatic changes in Eurasia and Africa at the last glacial maximum and mid-Holocene: reconstruction from pollen data using inverse vegetation modelling, *Clim. Dynam.*, 29, 211–229, <https://doi.org/10.1007/s00382-007-0231-3>, 2007.
- Yll, E. I., Pérez-Obiol, R., and Julià, R.: Vegetational change in the Balearic Islands (Spain) during the Holocene, *Hist. Biol.*, 9, 83–89, <https://doi.org/10.1080/10292389409380490>, 1994.
- Yll, E. I., Pérez-Obiol, R., Pantaleon-Cano, J., and Roure, J. M.: Dinámica del paisaje vegetal en la vertiente Mediterránea de la Península Ibérica e Islas Baleares desde el tardiglacial hasta el presente, in: *Reconstrucción Paleoambientes y cambios climáticos durante el Cuaternario*, edited by: Aleixandre, T. and Pérez-González, A. Higher Council for Scientific Research, 319–328, ISBN 84-00-07522-6, <https://dialnet.unirioja.es/servlet/libro?codigo=699264> (last access: 10 March 2023), 1995.
- Yll, E. I., Pérez-Obiol, R., Pantaleon-Cano, J., and Roure, J. M.: Palynological evidence for climatic change and human activity during the Holocene on Minorca (Balearic Islands), *Quaternary Res.*, 48, 339–347, <https://doi.org/10.1006/qres.1997.1925>, 1997.
- Zapata, L., Peña-Chocarro, L., Pérez-Jordá, G., and Stika, H.-P.: Early Neolithic Agriculture in the Iberian Peninsula, *J. World Prehist.*, 18, 283–325, 2004.
- Zhang, Y., Kong, Z., Ni, J., Yan, S., and Yang, Z.: Late Holocene palaeoenvironment change in central Tianshan of Xinjiang, northwest China, *Grana*, 46, 197–213, <https://doi.org/10.1080/00173130701564748>, 2007.